# Reduced-complexity Noncoherent Receiver for GMSK Signals

by

**Houhao Wang**

A thesis submitted in conformity with the requirements
for the degree of Master of Applied Science
Graduate Department of Electrical and Computer Engineering
University of Toronto

# Reduced-complexity Noncoherent Receiver for GMSK Signals

**Houhao Wang**

*A thesis submitted in conformity with the requirements for the Degree of Master of Applied Science, Graduate Department of Electrical and Computer Engineering, in the University of Toronto, 2001*

## Abstract

Gaussian Minimum Shift Keying(GMSK) is a spectrum and power efficient modulation scheme, used in many wireless communication systems. Since GMSK is nonlinear, the receiver for GMSK signals is more complex than that for linear modulation signals. A reduction in complexity can be achieved by employing a noncoherent signal detection scheme.

In this thesis, a reduced complexity noncoherent GMSK receiver, using the Laurent representation and noncoherent Decision Feedback Equalization(DFE), is proposed and evaluated first in an Additive White Gaussian Noise(AWGN) channel. The Bit Error Rate(BER) performance of the proposed receiver is compared to a corresponding coherent receiver. Furthermore, the proposed receiver is evaluated in static Finite Impulse Response(FIR) channels and multipath Rayleigh fading channels. The effects of two intrinsic parameters on performance are examined. It is concluded that the proposed receiver is a high performance noncoherent receiver when compared to other known noncoherent GMSK receivers.

# Acknowledgements

I am deeply grateful to my supervisor, Prof. S. Pasupathy, for his guidance and support throughout the course of my graduate studies. His numerous comments and careful reading of the manuscript are greatly appreciated.

I would like to thank Dr. R. Schober for his help and prompt replies to my questions.

I gratefully acknowledge the financial support I received in the form of the Ontario Graduate Scholarship, the University of Toronto Open Masters Fellowship and the research assistantship provided by Prof. S. Pasupathy.

Finally, I would like to thank my family for their patience, support and encouragement.

# Contents

# List of Figures

# List of Tables

# List of Acronyms

| | |
|---|---|
| AWGN | Additive White Gaussian Noise |
| T | Symbol Interval |
| GMSK | Gaussian Minimum Shift Keying |
| MSK | Minimum Shift Keying |
| ISI | Intersymbol Interference |
| LMS | Least Mean Square |
| LE | Linear Equalization/Equalizer |
| DFE | Decision Feedback Equalization/Equalizer |
| DFE(a,b) | DFE with x feedforward taps and b feedback taps |
| NDFE | Noncoherent DFE |
| BER | Bit Error Rate |
| PAM | Pulse Amplitude Modulation |
| CPM | Continuous Pulse Modulation |
| BPSK | Binary Phase Shift Keying |
| PSK | Phase Shift Keying |
| MMSE | Minimum Mean Square Error |
| MLSE | Maximum Likelihood Sequence Estimation |

| | |
|---|---|
| RLS | Recursive Lease Square |
| w | RLS weighting factor |
| rms | root mean square |
| FF | Feedforward |
| FB | Feedback |
| 1P | one-pulse |
| SNR | Signal to Noise Ratio |
| PSD | Power Spectral Density |

# Chapter 1

# Introduction

## 1.1 Motivation

The need for people to communicate with each other anytime, anywhere has greatly expanded the field of wireless communication. Due to users' demands for more and better wireless services, there is a need for higher transmission bandwidth. However, in a wireless communication system, adding bandwidth is not as easy as in a wire-line system. As a result, spectral congestion becomes a serious problem. A spectrally efficient modulation scheme, which maximize the bandwidth efficiency, is a very promising solution. To achieve spectral efficiency, certain modulation constraints are imposed, which lead to a more complex receiver design. As wireless communication becomes more popular, there is also a big demand for a more compact receiver. Therefore, there is a need to reduce the complexity of the receiver structures without losing much performance.

Gaussian Minimum Shift Keying(GMSK) is a spectrum and power efficient modulation scheme, used in many wireless communication systems. The GSM cellular, Cellular Digital Packet Data (CDPD) and Mobitex standards are some of the best known uses of GMSK. However, because of the phase modulation and Gaussian filtering, GMSK is not a linear modulation scheme. It is well known that the receiver

structure for a linear modulation scheme(e.g. Pulse Amplitude Modulation(PAM)) is less complex than that for the nonlinear modulation scheme. In addition, further complexity reduction can be achieved when noncoherent signal detection techniques are implemented. The goal of this thesis is to attempt to reduce the complexity of GMSK receiver by using a linear approximation of GMSK and noncoherent detection.

The reduction in demodulation complexity is achieved by using the Laurent representation of GMSK[31]. The Laurent representation decomposes Continuous Phase Modulation (CPM) signals into summations of PAM signals. It has been successfully implemented in [33], [34], and [35] to reduce the complexity of coherent CPM receivers. It is found that by using the main PAM pulse and a derotation process, the GMSK signals can be approximated by Binary Differential Phase Shift Keying(BDPSK) signals. Our challenge lies in designing a noncoherent GMSK receiver using the BDPSK approximation with sufficient performance in fading channels.

To improve the performance of the noncoherent receiver, Noncoherent Decision Feedback Equalization (NDFE) will be used. A high performance NDFE scheme is proposed by Schober et al.[29], for Phase Shift Keying (PSK) signal, in which the performance of the proposed NDFE scheme can approach the performance of the coherent DFE scheme in ISI channels. We will attempt to explore the use of this NDFE scheme for GMSK signals. The performance of the resulting noncoherent GMSK receiver will be compared to that of a corresponding coherent GMSK receiver.

Because we are interested in wireless applications, the proposed noncoherent receiver will be evaluated in static fading channels and quasi-static multipath Rayleigh fading channels. Since fading channels are harsher than the Additive White Gaussian Noise(AWGN) channel, it is expected that the performance of the receiver under fading channels will be worse than under the AWGN channel. Finally, the performance of the proposed receiver will be compared with other suitable noncoherent GMSK receivers.

## 1.2 Organization of Thesis

Chapter 2 presents a brief tutorial on GMSK, the Laurent representation, fading channel, GMSK signal detections and various equalization methods. Chapter 3 describes the design of reduced-complexity noncoherent GMSK receivers based on Laurent representation. Its performance in the AWGN channel will be compared to a corresponding coherent receiver. Chapter 4 examines the performance of the proposed noncoherent receiver under static fading channels and quasi-static multipath Rayleigh fading channels. Chapter 5 provides a summary and conclusions of this thesis along with suggestions for further research.

# Chapter 2

# Background and Literature Survey

This chapter gives a brief overview of GMSK and Laurent representation of Continuous Pulse Modulation(CPM). It also provides a review of signal detection schemes, fading channel and various receiver equalization strategies to combat intersymbol interference (ISI). Section 2.1 describes GMSK and its Laurent representation. Section 2.2 discusses receiver signal detection schemes. Section 2.3 introduces the multipath fading channel. Section 2.4 reviews the conventional adaptive equalization techniques for systems with coherent detection. Section 2.5 surveys the published literature on adaptive equalization techniques for systems with noncoherent detection.

## 2.1 GMSK and the Laurent Representation

### 2.1.1 GMSK

Gaussian Minimum Shift Keying belongs to the class of CPM schemes [1]. CPM is a modulation scheme in which the phase of the carrier is instantaneously varied by the modulating signal while the RF signal envelope is kept constant[1]. Due to the constant envelope, the CPM signals are not sensitive to amplifier nonlinearities, which results in a more compact power spectrum. The generation of CPM signals is shown in Figure 2.1 [1]. In the Figure, $\alpha[i]$ denotes the input sequence taken from

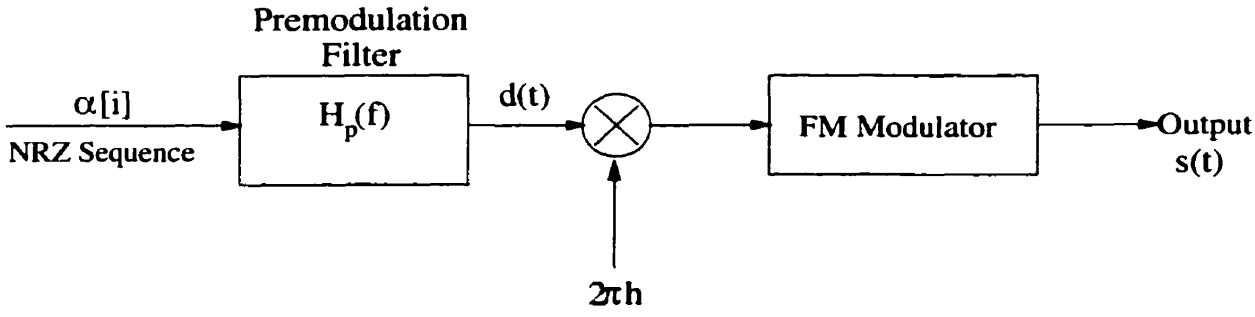


Figure 2.1: Block diagram of Continuous Phase Modulation

the M-ary alphabet $\pm 1$, $\pm 3$, $\pm(m-1)$ where $m = 2^k$, $k = 1, 2, 3....$ In this thesis, we only deal with the binary alphabet $\pm 1$. After passing through the pre-modulation filter with frequency response $H_p(f)$, the output signal d(t) can be expressed as

$$d(t) = \sum_{i=-\infty}^{\infty} \alpha[i] g(t - iT) \tag{2.1}$$

with $g(t) = h_p(t) \otimes p(t)$, where p(t) is a rectangular pulse of duration T and unity amplitude, $h_p(t)$ is the impulse response of the pre-modulation filter and "$\otimes$" denotes convolution. Mathematically, the transmitted signal $s(t)$ can be written as [1]:

$$s(t) = \sqrt{\frac{2E_s}{T}} \cos(2\pi f_c t + \phi(t, \alpha)) \tag{2.2}$$

where the phase function is expressed as

$$\phi(t, \alpha) = 2\pi h \int_{-\infty}^{t} \left( \sum_{i=-\infty}^{\infty} \alpha[i] g(v - iT) \right) dv \tag{2.3}$$

where $E_s$ is the transmitted energy per symbol, T is the symbol duration, h is the modulation index.

From (2.3), we observe that $\phi(t, \alpha)$ is a function of the integral of the pulse g(t). Let

$$q(t) = \int_{-\infty}^{t} g(v) dv$$

We can rewrite (2.3) as

$$\phi(t, \alpha) = 2\pi h \sum_{i=-\infty}^{\infty} \alpha[i] q(t - iT) \tag{2.4}$$

The phase function is a Pulse Amplitude Modulation(PAM) function with phase pulse q(t). Thus, the shape of g(t) determines the smoothness of the transmitted information carrying phase. The rate of change of the phase is proportional to h. By convention, the duration of g(t) is defined in number of bit duration,T. g(t) with duration LT, is normalized such that $\int_{-\infty}^{\infty} g(t)dt = 0.5$ [1]. For CPM schemes where g(t) has infinite duration, it will be truncated to some finite duration so as to contain most of the pulse energy.

For GMSK, h is 0.5 and the impulse response of the pre-modulation filter is a Gaussian function defined as:[1]

$$h_p(t) = B\sqrt{\frac{2\pi}{\ln 2}} \exp\left[-\frac{2\pi^2 B^2 t^2}{ln2}\right] \tag{2.5}$$

where B is the 3-dB bandwidth of the filter. By convention, B is normally expressed in terms of the inverse of T; therefore the 3-dB bandwidth of filter is defined as BT. The frequency pulse g(t) for GMSK is [35]:

$$f(t) = \frac{1}{2T}\left\{Q\left(2\pi B\frac{t-\frac{T}{2}}{\sqrt{ln2}}\right) - Q\left(2\pi B\frac{t+\frac{T}{2}}{\sqrt{ln2}}\right)\right\} \tag{2.6}$$

where

$$Q(t) = \int_t^{\infty} \frac{1}{\sqrt{2\pi}} \exp(\frac{-\tau^2}{2})d\tau$$

For GMSK, BT is used to control the bandwidth efficiency. In general, as BT decreases, the bandwidth efficiency increases. However, as BT decreases, g(t) spreads more in time and causes more ISI in (2.4). Therefore, for GMSK, there is a trade off between bandwidth efficiency and ISI. In the GSM standard, a BT of 0.3 is chosen. The resulting frequency and phase pulse is shown in Figure 2.2 along with some other BT values. As mentioned before, since g(t) has infinite duration, it has to be truncated. For BT=0.3, g(t) is truncated to a duration of 3T.

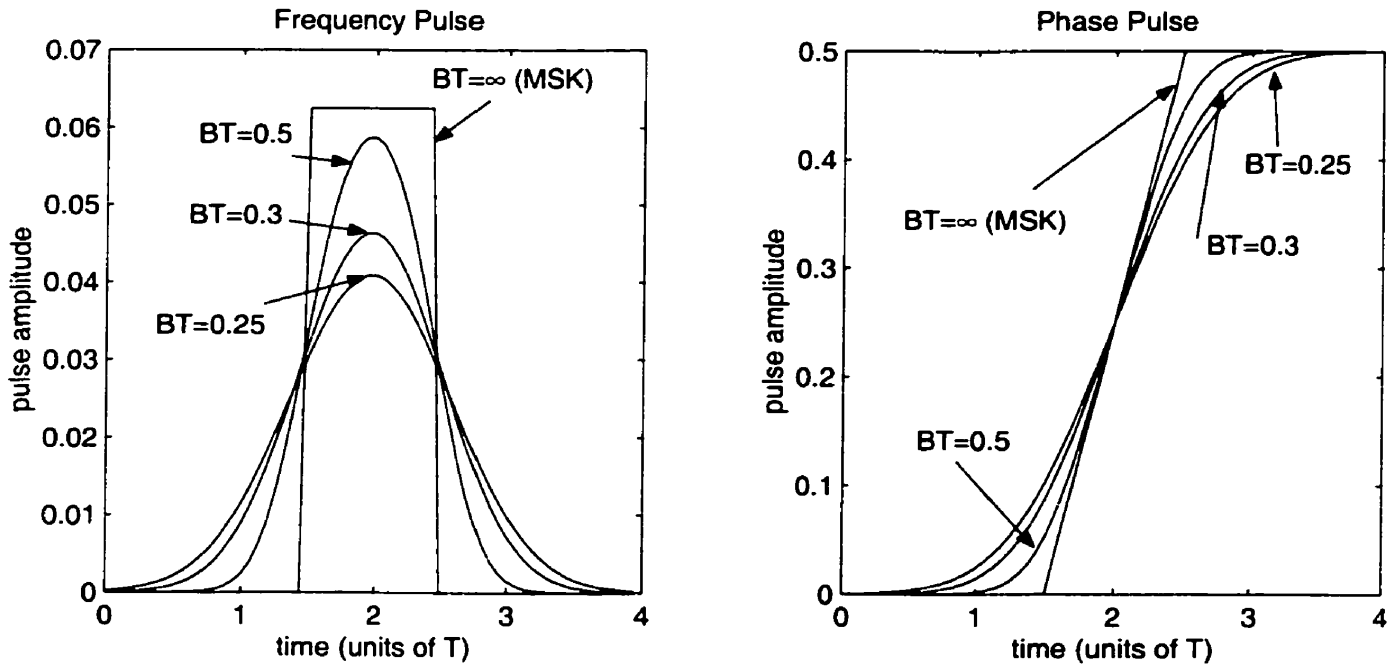


Figure 2.2: GMSK frequency and phase pulses for various BT

### 2.1.2 The Laurent Representation of CPM

In baseband, CPM signals can be represented as $s(t) = e^{j\phi(t,\alpha)}$, where $\phi(t,\alpha)$ is given by (2.4). For $nT \leq t \leq nT + T$, we have

$$e^{j\phi(t,a)} = \exp\left(j\pi h \sum_{i=0}^{n-L} \alpha[i]\right) \prod_{i=n-L+1}^{n} \exp[j\pi h\alpha[i]q(t-iT)] \tag{2.7}$$

Let $J = \exp(j\pi h)$, then $J^{\alpha[i]} = cos(\pi h) + j\alpha[i]sin(\pi h)$. Using this relation, the product terms of (2.7) can be expressed as

$$\begin{aligned}\exp[j\pi h\alpha[i]q(t-iT)] &= cos[\pi hq(t-iT)] + j\alpha[i]sin[\pi hq(t-iT)] \\ &= J^{\alpha[i]}\frac{sin[\pi hq(t-iT)]}{sin(\pi h)} + \frac{sin[\pi h - \pi hq(t-iT)]}{sin(\pi h)}\end{aligned} \tag{2.8}$$

If we also notice that $1 - q(t) = q(LT) - q(t) = q(LT - t)$ and define

$$B(t) = \begin{cases} \frac{\sin(\pi h - \pi hq(t))}{sin\pi h} : & 0 \leq t \leq LT \\ B(-t) : & -LT \leq t \leq 0 \end{cases}$$

$$a_0[n-L] = \exp\left(j\pi h \sum_{i=0}^{n-L} \alpha[i]\right)$$

we have

$$s(t) = a_0[n-L] \prod_{i=n-L+1}^{n} [J^{\alpha[i]} B(t-iT-LT) + B(t-iT)] \tag{2.9}$$

Expanding (2.9), Laurent [31] shows that there are only $2^{L-1}$ different pulses and each pulse is obtained by the product of L shifted version of B(t). For binary GMSK(h=0.5, J=j), it can be shown that the Laurent representation is given by

$$s(t) = \sum_{i=0}^{2^{L-1}-1} \sum_{n=-\infty}^{\infty} a_i[n] h_i(t-nT) \tag{2.10}$$

where $h_i(t)$ terms are the impulse responses of the Laurent PAM pulses and

$$a_0[n] = a_0[n-1] j^{\alpha[n]}$$

$$a_i[n] = a_0[n-L] \prod_{i \in I_k} j^{\alpha[n-i]}$$

where $I_k$ is a nonempty subset of the set $\{0, 1, ..., L-1\}$. The Laurent representation of GMSK modulator and its corresponding optimum receiver is derived in [33] and shown in Figure 2.3 and Figure 2.4. It is shown that an optimum coherent Laurent-based MLSE GMSK demodulator requires $4 \times 2^{L-1}$ states. For GMSK with BT=0.3 and L=3, 16 states are needed. The BER performance of the optimum MLSE GMSK receiver under AWGN channel is shown in Figure 2.5. However, it is noted in [32] that the main Laurent pulse, $h_0$, contains most of the GMSK signal energy. By using only $h_0$, the author proposed a reduced complexity coherent MLSE demodulator with 4 states. Compared to the optimum receiver, it only suffers around 0.3 dB SNR performance loss under AWGN channel. Here, SNR is defined as:

$$SNR = 10log_{10} \frac{E(||s(t)||^2)}{E(||n(t)||^2)}$$

where $s(t)$ is the transmitted signal, $n(t)$ represents complex additive Gaussian noise with a one-sided power spectral density of $N_0$. Thus, in this work, we will use only the main pulse, $h_0$.

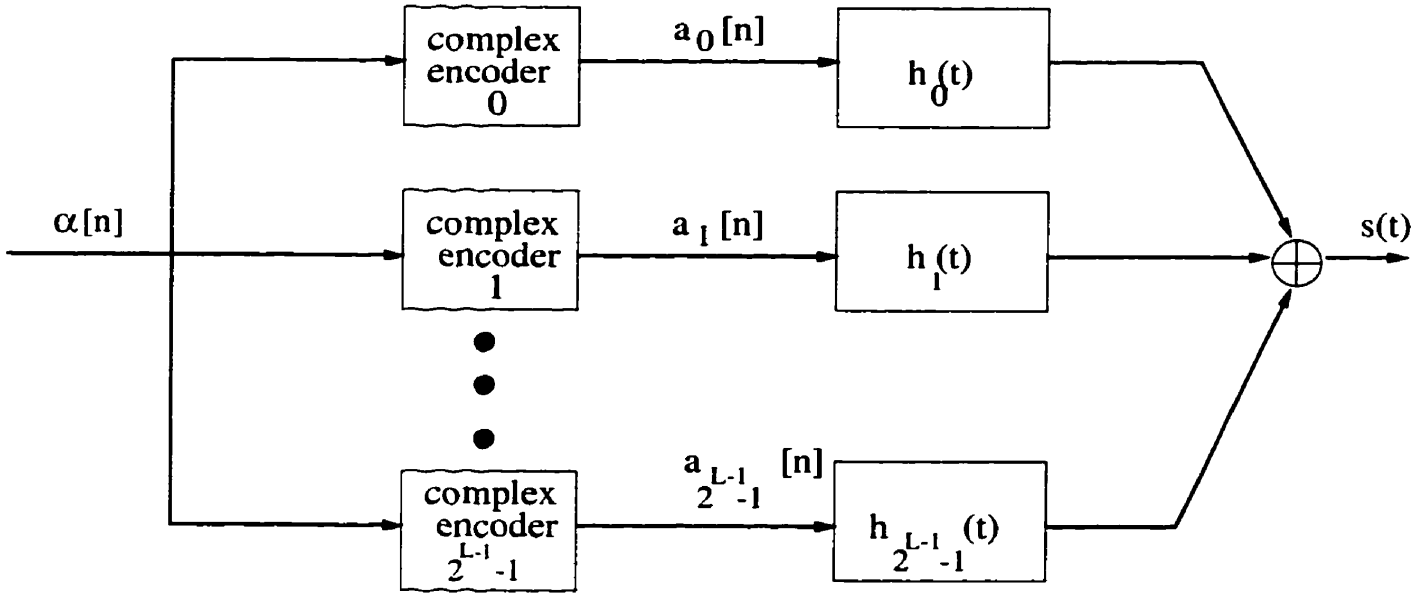


Figure 2.3: Laurent representation of a GMSK modulator

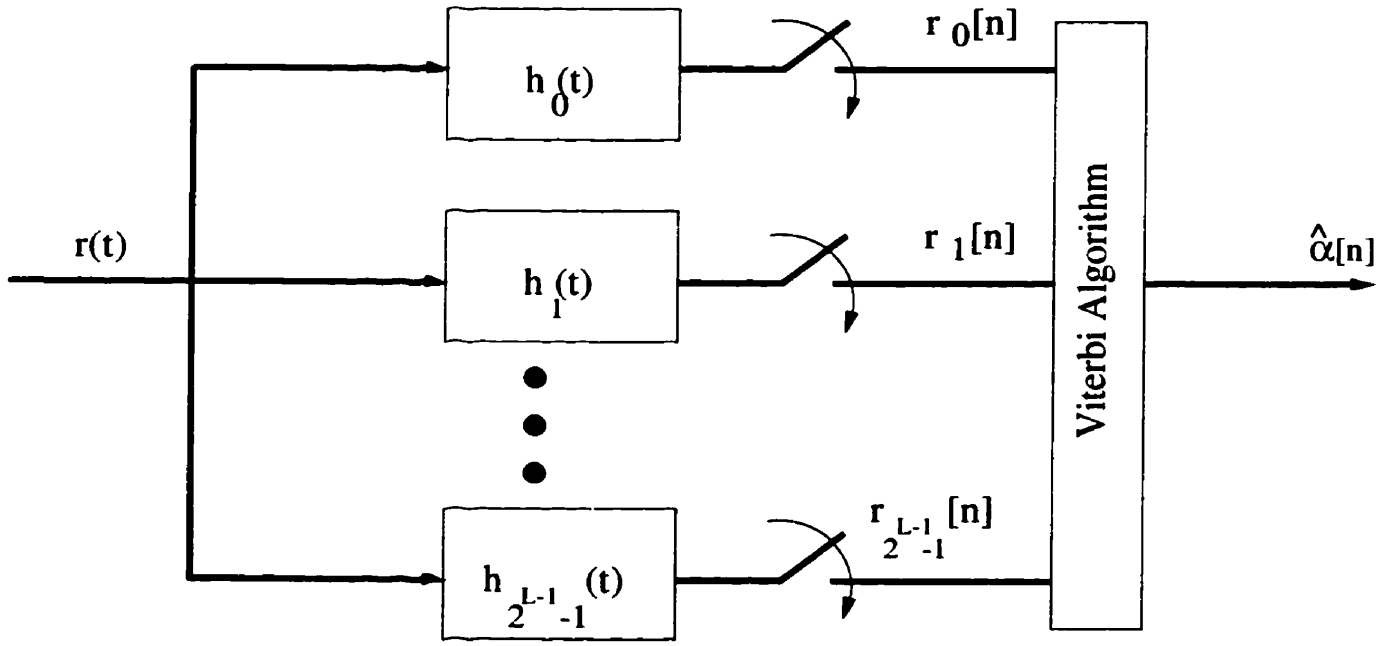


Figure 2.4: Optimum Laurent-based demodulator

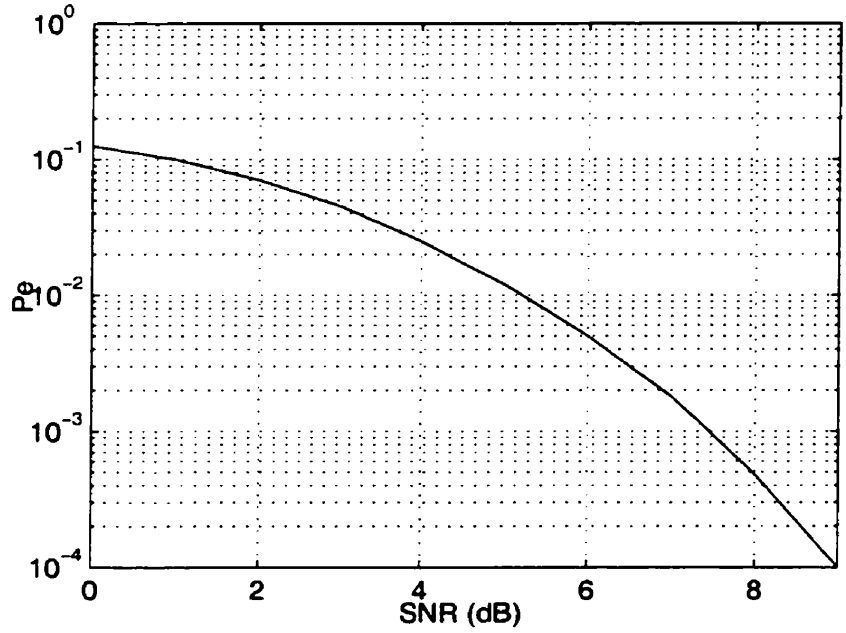


Figure 2.5: Performance of the optimum Laurent receiver for GMSK with BT=0.3 [32]

## 2.2 Signal Detection

There are two general methods to detect the received signal. One method requires estimation of the carrier phase $\phi = 2\pi f_c t_o$ at the receiver, where $t_o$ is the time delay and $f_c$ is the carrier frequency. The estimated $\phi$ is needed to compensate for the channel phase shift. This type of detection is called coherent detection. In a typical coherent detection system, pilot tones[9] are transmitted at a convenient frequency in the data spectrum. It is extracted at the receiver and the channel impairment can then be deduced from the received tone. The information from the channel can assist in the reconstruction of a coherent reference signal. A coherent detector for GMSK is shown in [6].

The other method ignores $\phi$ in the detection process and is called noncoherent detection. There are two major subdivisions of noncoherent detection:limiter/discriminator [10] [11] [13] and differential detection[14] [15]. Limiter/discriminator has a hard lim-

iter followed by a bandpass filter. The limiter is used to remove the amplitude noise of the received signal [17]. The resulting signal is a constant-envelope sinusoid and is demodulated by the discriminator. In differential detection, instead of using absolute carrier phase, information is encoded using the carrier phase differences. At the receiver, it is then recovered by obtaining the difference in phase of received signal at current time and at past time, usually at multiples of the symbol period. Because only the phase difference of the carrier is used in the transmission and detection, the need for carrier recovery is eliminated.

Since the noncoherent detection does not need to generate a carrier reference at the receiver, noncoherent detectors are simpler to implement than coherent detectors. Although coherent detection performs generally better than noncoherent detection, noncoherent detection performs better in severe fading channels[14]. This is because under fading conditions, it is difficult to precisely regenerate the reference carrier needed in coherent detection. Among the noncoherent detection schemes, a major disadvantage of the limiter/discriminator approach is that it suffers from the FM threshold effect when the signal carrier to noise ratio falls below a certain level[17]. Differential detection does not suffer from the threshold effect. It is affected only by severe channel delay distortion [18]. In addition, differential detection improves performance by canceling the phase distortion between adjacent symbols during phase subtraction. In the case of GMSK, the inherent ISI due to pulse shaping can be partially eliminated with decision feedback[15].

## 2.3 Multipath Fading Channel

There are two types of fading effects that characterize wireless channels: large-scale and small-scale fading. Large-scale fading represents the average signal power attenuation or path loss due to motion over large areas.[4] It is mainly affected by prominent terrain contours(hill, forests, buildings, etc.) between the transmitter and receiver.

When under large-scale fading, the receiver is often referred to as being "shadowed" by such prominence. Small scale fading is used to describe the rapid fluctuation of the amplitude of a radio signal over a short period of time or travel distance, so that large-scale fading effects may be ignored. This thesis only deals with small-scale fading.

In wireless communication channels, the transmitted RF wave travels to the receiver through multiple reflective paths. The channel in which the transmitted signal propagates via multiple paths is called a multipath channel. With each path, there exists an attenuation factor and a propagation delay. The attenuation factor accounts for the amplitude variations in each multipath component and the propagation delay accounts for the phase variations. Due to the constructive and destructive interferences of these components at the receiver, the received signals can vary widely in amplitude and phase. Multipath fading occurs when the receiver undergoes destructive interference. The severity of fading mainly depends on the distribution of the intensity and relative propagation time of the RF waves and the bandwidth of the transmitted signal[5].

To characterize the multipath fading channel, a set of channel correlation functions and power spectra can be used[5]. The characterization can be classified according to the time variations of the channel and the frequency variations of the channel. The time variations of the channel is measured by the Doppler spread and the coherence time. The Doppler spread is the width of the Doppler spectrum, caused by the Doppler effect. It represents the strength of the Doppler shift at different frequencies[5]. The coherence time, $t_c$ is approximately equal to the reciprocal of Doppler spread and is a measure of the time interval over which the channel conditions remain approximately constant. If the coherence time of the channel is smaller than the symbol period of the transmitted signals, the signals are undergoing fast fading. Fast fading causes frequency dispersion which leads to signal distortion. Fast fading is also called time selective fading. In this thesis, we will assume that the sym-

bol period is small enough compared to the coherence time such that the channel is not time selective(slow fading). The frequency variations of the channel can be measured by the coherence bandwidth and the multipath delay spread. The coherence bandwidth, $\Delta f_c$ is a measure of the bandwidth over which the signals in frequency will be affected similarly by the channel. The reciprocal of $\Delta f_c$ is approximately equal to the multipath delay spread, which is a measure of the time dispersion of a transmitted signal caused by the channel[5]. If the coherence bandwidth is smaller than the bandwidth of the transmitted signal waveform, the signals are undergoing frequency selective fading. Frequency selective fading is caused by the time dispersion of the transmitted symbols within the channel, and therefore, the channel induces ISI[5].

## 2.4 Equalization for A Coherent System

One of the major obstacles to high speed data transmission over wireless channels is ISI[5]. The ISI caused by multipath in a time dispersive channel distorts the transmitted signal, causing bit errors at the receiver. Equalization is a signal processing technique used to combat ISI. Depending on the transmission channel and application, there are many equalization schemes to choose from. We present several main ones in this section.

### 2.4.1 Maximum Likelihood Sequence Estimation

Equalization based on the maximum likelihood sequence detection (MLSD) criterion is the optimum scheme in the view of probability of sequence error[3]. From [2], we see that the ISI observed at the output of the demodulator may be viewed as the output of a finite state machine. This implies that the channel output with ISI may be represented by a trellis diagram, and the maximum likelihood estimate of the received data sequence is simply the most probable path through the trellis given the received demodulator output sequence. Viterbi algorithm provides an efficient way to

search the trellis. However, the size of states for the equivalent finite state machine grows exponentially with the length of the channel time dispersion. If the size of the symbol alphabet is M and the number of interfering symbols contributing to ISI is L, the Viterbi algorithm computes $M^{L+1}$ metrics for each new received symbol [2]. For frequency selective channels, the ISI may span many symbols. The computational complexity of the MLSE will be too high to implement. Therefore, suboptimum channel equalization schemes must be used.

### 2.4.2 Linear Transversal Equalization

Unlike MLSD equalization, the linear transversal equalization structure has a computational complexity that is a linear function of the channel dispersion length L. It is the simplest equalization structure, Figure 2.6 shows a block diagram of the linear equalizer[3]. For linear equalizer, the current and past values of the received signal

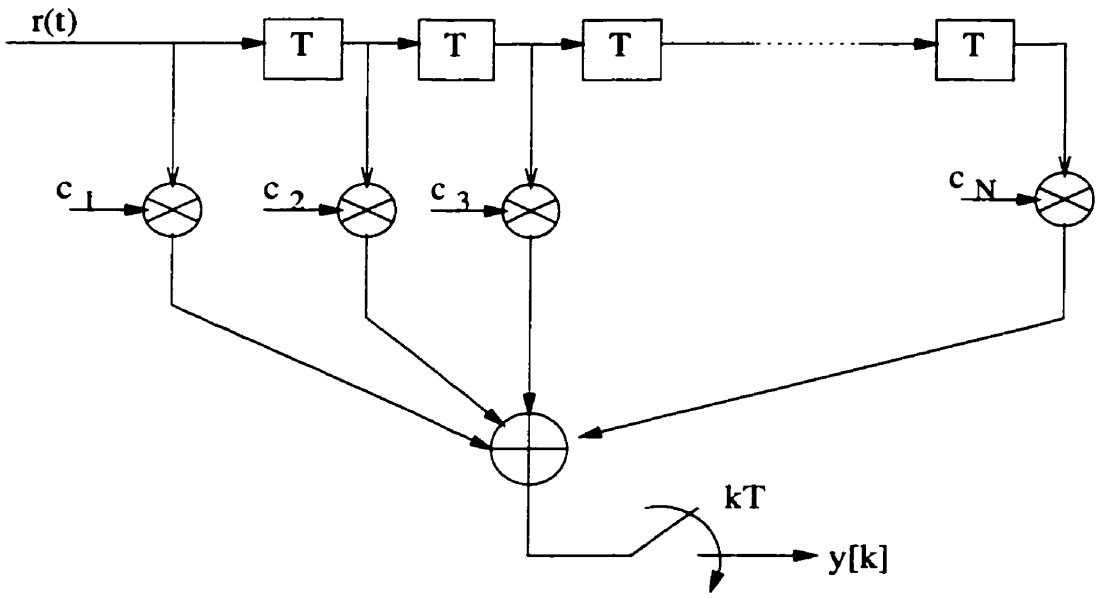


Figure 2.6: Linear transversal equalizer

are linearly weighted by equalizer coefficients $c_n$ and summed to produce the output. When implemented digitally, the samples of the received signal at the symbol rate

are stored in a digital shift register, and the equalizer output samples $y[k]$ can be expressed as:

$$y[k] = \sum_{n=1}^{N} c_n r(kT - nT) \tag{2.11}$$

where N is the number of equalizer coefficients. The equalizer coefficients, $c_n$ may be chosen to force the samples of the combined channel and equalizer impulse response to zeros at all but one of the N T-spaced instants in the span of the equalizer. Such an equalizer is called a zero-forcing(ZF) equalizer[3]. If the number of coefficients of a ZF equalizer increase to infinity, there would be no ISI at its output. It is shown in [3] that an infinite length zero-forcing ISI equalizer is simply an inverse filter, which inverts the folded frequency response of the channel. A finite length ZF equalizer approximates this inverse. However, such an inverse filter may excessively enhance noise at frequencies where the folded channel spectrum has high attenuation. This is undesirable, particularly for frequency selective fading channels.

### 2.4.3 Decision Feedback Equalization

Decision Feedback Equalization(DFE) is another simple suboptimal equalization scheme that is very useful for channels with severe amplitude distortion. The DFE consists of a feedforward filter and a feedback filter that are similar to the linear equalizer. The idea here is that if the value of the symbols already detected are known(and assumed to be correct),then the ISI contributed by these symbols can be canceled exactly, by subtracting past symbol values with appropriate weighting from the equalizer output. Figure 2.7 shows a DFE [2]. Here, the output of the equalizer can be expressed as:

$$\hat{I}[k] = \sum_{j=-K_1}^{0} c_j v[k-j] + \sum_{j=1}^{K_2} c_j \tilde{I}[k-j] \tag{2.12}$$

where $\hat{I}[k]$ is an estimate of the kth information symbol, $c_j$ are the tap coefficients of the filter, and $\tilde{I}[k-1], ...., \tilde{I}[k-K_2]$ are previously detected symbols. The equalizer is assumed to have $(K_1 + 1)$ taps in its feedforward section and $K_2$ in its feedback section. Since the feedback filter contains previously detected symbols, this equalizer

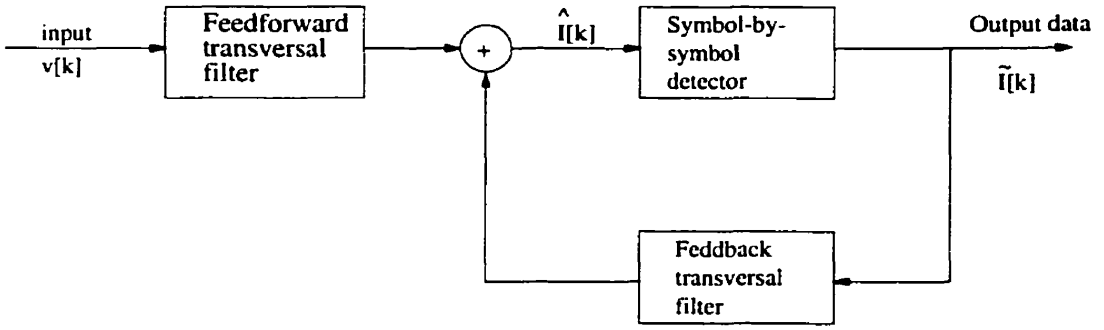


Figure 2.7: Decision feedback equalizer

is clearly nonlinear. By assuming that previously detected symbols in the feedback filter are correct, the minimization of Mean Square Error(MSE)[2]:

$$J(K_1, K_2) = E|I[k] - \hat{I}[k]|^2 \tag{2.13}$$

leads to the following set of linear equations for the coefficients of the feedforward filter:

$$\sum_{j=-K_1}^{0} \psi_{lj} c_j = f_{-l}^*, \quad l = -K_1, ...., -1, 0 \tag{2.14}$$

where $f_l$ is a set of tap coefficients used to model the ISI channel.

$$\psi_{lj} = \sum_{m=0}^{-l} f_m^* f_{m_l - j} + N_o \delta_{lj}, \quad l, j = -K_1, ...., -1, 0 \tag{2.15}$$

The coefficients of the feedback filter of the equalizer are given in terms of the coefficients of the feedforward section by the following expression:

$$c_k = -\sum_{j=-K_1}^{0} c_j f_{k-j}, \quad k = 1, 2, ..., K_2 \tag{2.16}$$

The values of the feedback coefficients result in complete elimination of ISI from previously detected symbols, provided that previous decisions are correct. However, due to the feedback, in a practical DFE, decision errors may propagate. Fortunately, the propagation is not catastrophic and generally, errors occur in short bursts that degrade the performance only slightly[2].

### 2.4.4 Adaptive Equalization

In wireless communication systems, the channel characteristics are unknown and the channel response is time-variant. Thus, the equalizers must be designed to be adjustable to the changing channel response. Both linear equalization and DFE discussed so far can be made adaptive with some modification[2]. Since this thesis deals with DFE, we will focus on adaptive DFE. For adaptive DFE, the filter coefficients $c_j$ are adjusted recursively in order for the filter to track time variations in the channel response. For this purpose, an error signal is formed by taking the difference between the detected symbol $\tilde{I[k]}$ and the estimate $\hat{I}[k]$, i.e.$\varepsilon_k = \tilde{I}[k] - \hat{I}[k]$.[2] The error signal is then scaled by a factor $\Delta$ and the resulting product is used to adjust the coefficients base on the minimization of the MSE at the output of the DFE by using the steepest-descent algorithm[2].

$$\hat{C}[k+1] = \hat{C}[k] + \Delta E(\varepsilon[k]\tilde{V}[k]^*) \tag{2.17}$$

where $\hat{C}[k]$ is the vector of tap gain coefficients in the kth signaling interval,$E(\varepsilon[k]\tilde{V}[k]^*)$ is the cross-correlation of the error signal $\varepsilon[k]$ with the vector $\tilde{V}[k]$ with component $(v[k+K_1], ..., v[k], \tilde{I}[k-1], ..., \tilde{I}[k-K_2])$. $\tilde{V}[k]$ represents the signal values in the feedforward and feedback filters at time $t = kT$. The MSE is minimized when $E(\varepsilon[k]\tilde{V}[k]^*) = 0$ as $k \to \infty$. However, at any time instant, the exact cross-correlation vector is unknown[2]. We can estimate the vector $\varepsilon[k]\tilde{V}[k]^*$ and average out the noise in the estimate. This gives us the least-mean-square(LMS) algorithm for DFE:

$$\hat{C}[k+1] = \hat{C}[k] + \Delta\varepsilon[k]\tilde{V}[k]^* \tag{2.18}$$

where $\Delta$ is the step size. The larger the step size, the faster the equalizer tracking capability and the greater the excess MSE. Thus, a compromise must be made between fast tracking and excess MSE of the equalizer. The excess MSE is the part of the error power in excess of the minimum attainable MSE.[3] It is caused by tap weights wandering around their optimum settings. The excess MSE is directly proportional

to the number of equalizer coefficients, the step size, and the channel noise power.[3] To initialize the DFE tap weights, a known information sequence(training sequence) is transmitted to the receiver. This is the training mode of the DFE. The training is finished when the equalizer coefficients converge to the optimum value(minimum MSE). Then, the DFE can be switched to the decision-directed mode where the real data sequence can be used. The main advantage of the LMS algorithm is computational simplicity and the main drawback is the slow convergence rate. Many other algorithms have been developed to improve convergence speed by trading off computational complexity. Recursive Least Square(RLS) algorithm is one such well known algorithm. Thus, it will be used in this thesis. Unlike LMS, RLS algorithm requires the generation of the coefficient vector $c_n$ at time n to minimize the sum of all squared errors as if $c_n$ were used over all the past received signal[3]. In order to permit tracking of slow time variations, a decay factor $w$ with a value slightly less than unity is introduced. The DFE tap gain coefficients can be generated recursively according to

$$\hat{C}[k+1] = \hat{C}[k] + \hat{K}[k]\varepsilon[k] \tag{2.19}$$

where $\varepsilon[n]$ is the equalizer output error and $\hat{K}[k]$ is the Kalman gain vector. The Kalman algorithm is used to recursively compute the Kalman gain[3].

### 2.4.5 Fractionally Spaced Equalization

So far, the delay taps of the discussed equalization structures are spaced at the reciprocal of the symbol rate, 1/T. This tap spacing is optimum if the equalizer is preceded by a filter matched to the channel distorted transmitted pulse[3]. When the channel characteristics are unknown, the receiver filter is usually matched to the transmitted signal pulse and the sampling time is optimized for this filter. This approach leads to an equalizer performance that is very sensitive to the choice of sampling time. As a solution, fractionally spaced equalization(FSE) can be implemented. FSE can be applied to both linear equalization and DFE. A fractionally spaced linear equaliza-

tion structure is shown in Figure 2.8[3]: where the delay line taps are spaced at an

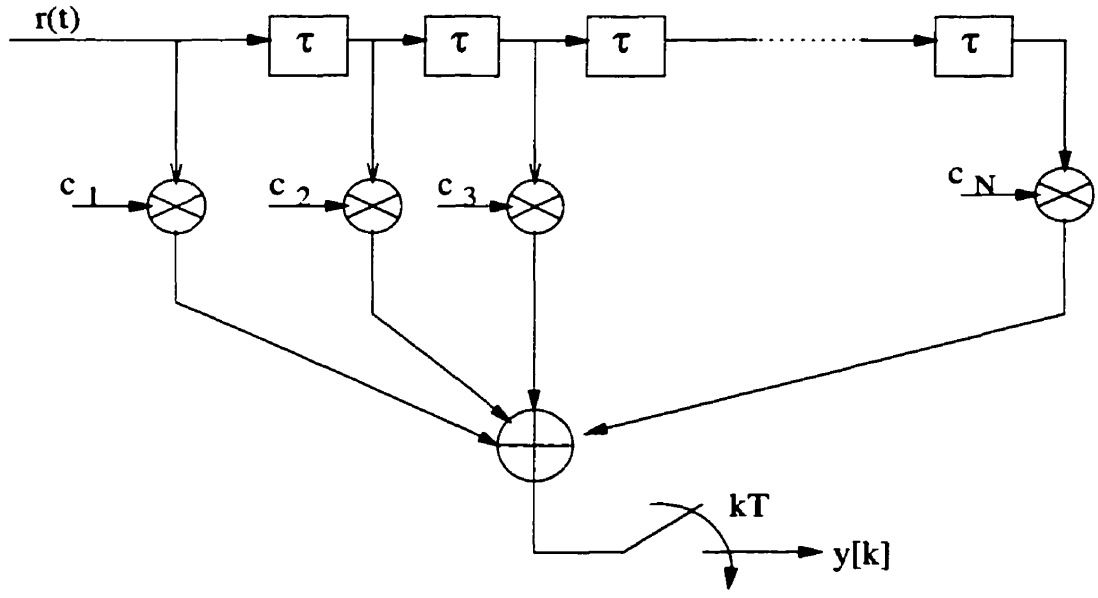


Figure 2.8: Fractionally spaced linear equalizer

interval $\tau$ which is less than the symbol interval T. $\tau$ is typically selected such that the bandwidth occupied by the signal at the equalizer input satisfies the sampling theorem. In digital implementation, $\tau$ is selected to be AT/B where A and B are integers and $B > A$. The equalization output is given by

$$y[k] = \sum_{n=1}^{N} c_n r\left(kT - \frac{nAT}{B}\right) \tag{2.20}$$

The adaptive algorithms discussed in section 2.4.4 can also be used for FSE. As an example, the LMS algorithm(2.18) can now be written as:

$$\hat{C}[k+1] = \hat{C}[k] + \Delta\varepsilon[k]r^*\left(t_0 + kT - \frac{nAT}{B}\right) \tag{2.21}$$

Because of the higher sampling rate, FSE can effectively compensate for more severe delay distortion and deal with amplitude distortion with less noise enhancement than a T spaced equalizer.

## 2.5 Equalization for Noncoherent Systems

The implementation and operation of coherent detection is a complex process involving many ancillary functions associated with the carrier synchronization loop, for example, acquisition, tracking, lock detection, etc. In many applications, it is more desirable to have simple and robust implementation than have the best possible system performance. Therefore, noncoherent detection schemes are more attractive. In this thesis, we will use differential detection. Since the nonlinear nature of differential detection and the presence of frequency selective fading channels make linear equalization a less than satisfactory choice, Noncoherent DFE(NDFE) will be considered. We will now discuss some of the known NDFE schemes.

A noncoherent equalizer for DQPSK under frequency-selective mobile radio channels with differential detection is proposed by Kohama et al.[24]. A block diagram of the receiver is shown in Figure 2.9. This equalizer adjusts the decision thresholds

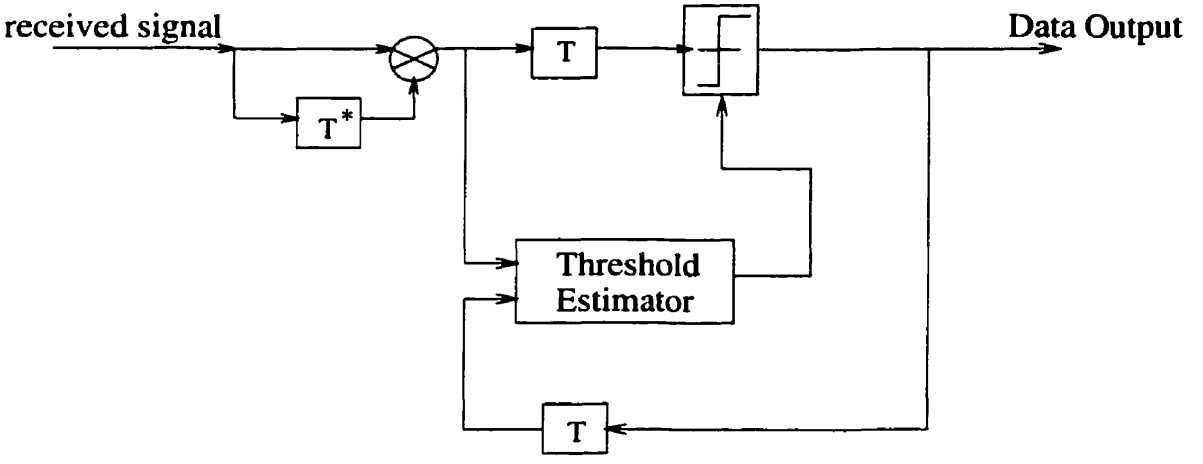


Figure 2.9: Block diagram of the RAM based equalizer

adaptively by decision feedback. The threshold control signal is stored in a Random Access Memory(RAM) during the training period. As the training signal starts, the signals are sampled and stored. The sampled signals are mapped in a complex plane. Decision boundaries are drawn to separate four signal points and stored in the

threshold data RAM. Because the transmitted training data is known, it is possible to determine which region corresponds to a data signal among the four signal points. The result is then written in a classifying RAM. The information data can then be determined by finding out which region the sampled information signal falls in the classifying RAM.

The performance of an indoor radio system with DQPSK modulation in frequency selective fading channels has been studied by Benvenuto et al.[25]. Based on the nonlinear echo canceler given in [26], a nonlinear equalizer is proposed with differential detection. A block diagram of the receiver is shown in Figure 2.10. The structure

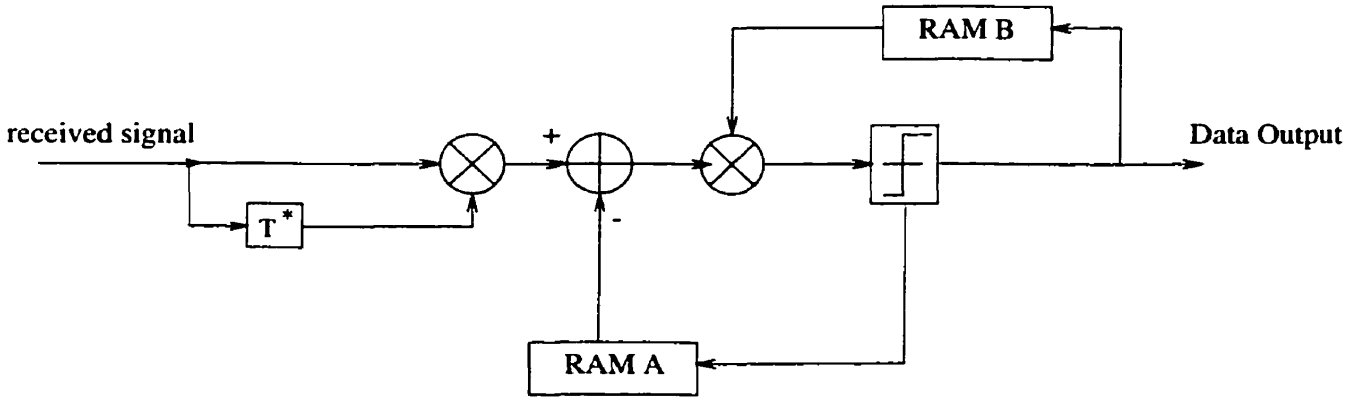


Figure 2.10: Block diagram of another RAM based equalizer

of the filter taps of the proposed equalizer is based on the table look-up method which takes the form of RAMs. The update of the coefficients is achieved by adding a scaled portion of error signal to the current RAM contents. The equalizer employ two RAMs; one for removing the nonlinear ISI due to the multiplication in the differential detector and the other one for compensating the additive interference. The content of each RAM location is determined by making use of a training sequence. The equations for updating the RAM locations are based on the LMS algorithm. Since [24] and [25] both employ RAMs, they are not robust compared to conventional DFE when various channels are considered.

A more robust NDFE structure is proposed by Masoomzadeh-Fard et al. for

Differential Phase Shift Keying(DPSK) under multipath fading channels[27]. The Noncoherent receiver is illustrated in Figure 2.11[27]. In the Figure, $r_k$ is the received

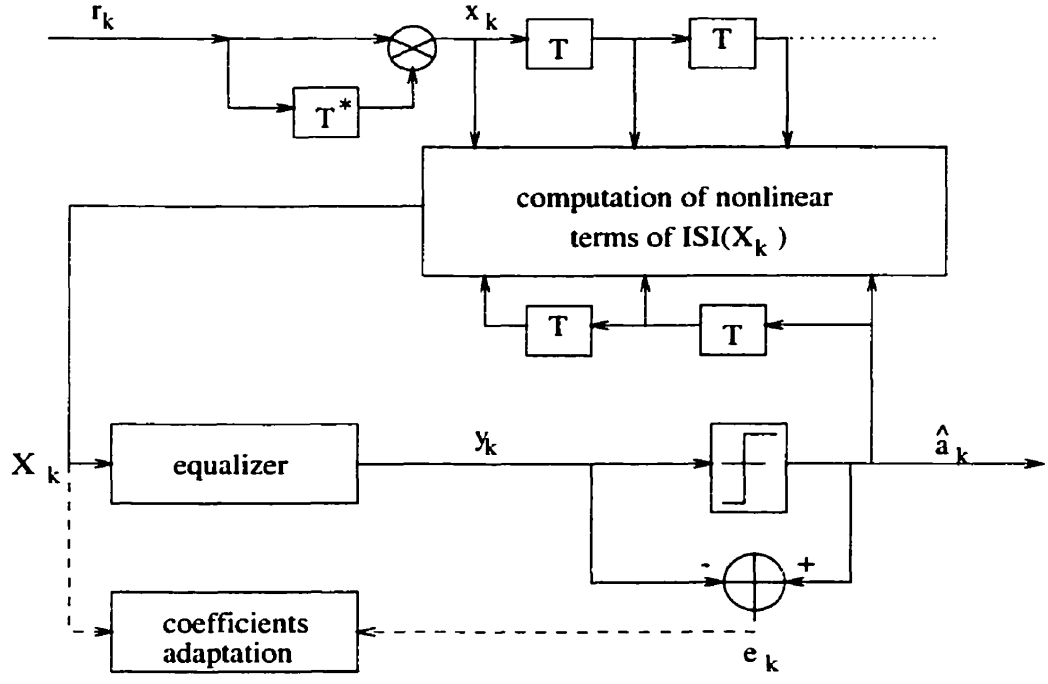


Figure 2.11: A noncoherent decision feedback equalizer

signal(after T sampling), which has been differentially encoded at the transmitter. After receiving $r_k$, a conventional differential detector is applied to remove the absolute phase of the received signal. In the next stage of the receiver, the nonlinear ISI caused by differential detection is calculated by using decision feedback. They are then weighted and summed in a conventional equalizer. Finally, the equalizer output is quantized to form the decision $\hat{a_k}$, which should be equal to the original transmitted symbol $a_k$ if no error occurs. In addition, it is shown that for nonlinear phase channels, the differential detector creates large amounts of phase distortion and therefore, a T-spaced nonlinear equalizer is unable to equalize these channels. The authors proposed a fractionally-spaced NDFE structure which significantly outperforms the T-spaced NDFE structure. However, in the proposed NDFE algorithm, a nonlinear processor with $O(L^2)$ complexity is used to determine the elements in the

equalizer input vector, where $L$ is the number of significant symbol-spaced multipath components in the channel[28]. Jones et al. [28] used the same NDFE structure, but provided a more computationally efficient DFE algorithm. However, the proposed NDFE structure is suboptimum and cause a large loss in power efficiency(typically more than 4 dB) when compared with coherent DFE[29]. Schober et al. [29] proposed a high performance NDFE scheme for the ISI channel. This scheme is derived from optimum noncoherent MLSE and can approach coherent Minimum Mean Square Error (MMSE) DFE arbitrarily close[29]. So far, no other combination of an equalizer and a noncoherent detector has been reported in literature, which can approach the performance of a corresponding coherent receiver[30]. For adaptation of the feedforward and feedback filters, efficient novel modified Least Mean Square(LMS) and Recursive Least Square(RLS) algorithms are provided. Simulations confirm that the proposed adaptive NDFE schemes are robust against frequency offset. The details of this NDFE scheme will be further described in the following chapter.

# Chapter 3

# Demodulating GMSK with Adaptive DFE in AWGN Channel

The previous chapter gives an overview on GMSK, the Laurent representation of CPM, signal detection schemes, fading channel and some typical coherent and noncoherent equalization techniques. We learned that due to its low implementation costs and robustness against frequency and carrier phase offsets, differential detection, a noncoherent signal detection schemes, is can be more advantages over coherent signal detection schemes in a fading channel. In addition, we learned that under severe fading channel, such as channels with spectral null, DFE is a better suboptimum equalization technique than LE.

This chapter discusses the design issues of a noncoherent GMSK receiver based on the Laurent representation under AWGN channel. Section 3.1 derives a reduced complexity PSK-based GMSK demodulator. Section 3.2 discusses the use of coherent DFE with the GMSK demodulator. The BER performance of the overall coherent receiver structure will be used as the performance benchmark. Section 3.3 discusses the use of noncoherent DFE with the GMSK demodulator. Section 3.4 discusses the use of fractionally spaced DFE with the GMSK demodulator. For convenience of simulation, we will use GMSK with Global System Mobiles(GSM) standard, which

specifies a BT of 0.3. Thus, we truncates the GMSK frequency pulse to 3T.

## 3.1 The Laurent Approximation of GMSK Signals

It was shown by Laurent [31] that any binary CPM signal with modulation filter duration L can be written as a sum of $2^{L-1}$ PAM signals. By applying this result, we can write the transmitted GMSK signals with BT=0.3 and L=3 as the sum of four PAM modulated signals:

$$s(t) = \sum_{k=0}^{3} \sum_{n=-\infty}^{\infty} a_k[n] h_k(t - nT) \tag{3.1}$$

where k is the PAM pulse index, n is the index of the current bit of the input sequence, and

$$\begin{aligned} a_0[n] &= a_0[n-1] j^{\alpha[n]} \quad \text{with,} \\ j &= e^{j\frac{\pi}{2}} \quad \text{and} \quad \alpha[n] \in 1, -1 \end{aligned} \tag{3.2}$$

The other $a_k[n]$ have the following general form:

$$\begin{aligned} a_k[n] = a_0[n-3] \prod_{i \in I_k} j^{\alpha[n-i]}, \quad k = 1, 2, 3 \\ \text{with, } I_k \subset \{0, 1, 2\} \end{aligned} \tag{3.3}$$

The PAM pulses are expressed as:

$$\begin{aligned} h_0(t) &= B(t-3T)B(t-2T)B(t-T): \quad 0 \le t \le 4T \\ h_1(t) &= B(t-3T)B(t+T)B(t-T): \quad 0 \le t \le 2T \\ h_2(t) &= B(t-3T)B(t+2T)B(t-2T): \quad 0 \le t \le T \\ h_3(t) &= B(t-3T)B(t+2T)B(t+T): \quad 0 \le t \le T \end{aligned}$$

where, $B(t)$ is defined as:

$$B(t) = \begin{cases} \sin(\frac{\pi}{2}(1 - q(t))): & 0 \le t \le 3T \\ B(-t): & -3T \le t \le 0 \end{cases} \tag{3.4}$$

$q(t)$ is the GMSK phase shaping filter discussed in Chapter 2. Numerical integration of the main Laurent pulse, $h_0$, shows that it contains 99.7% of the total GMSK pulse energy. Thus, $s(t)$ can be well represented in terms of $h_0(t)$ only. The pulse shape for $h_0$ is shown in Figure 3.1. Note that although $h_0$ is defined over 4T, the main

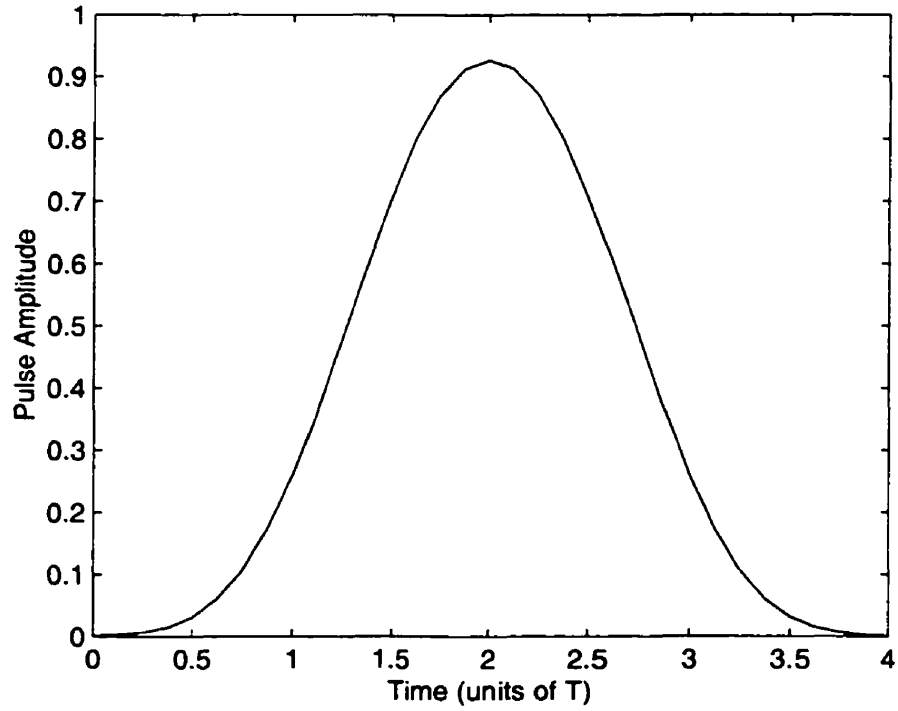


Figure 3.1: The Laurent main pulse

pulse energy is contained within 3T. $h_0$ can then be truncated to 3T. By using only $h_0$, $s(t)$ can be further simplified to:

$$s(t) \approx \sum_{n=-\infty}^{\infty} a_0[n] h_0(t - nT) \tag{3.5}$$

From (3.2), if we assume that the initial state of $a_0[n] = 1$ and note that $j^{\alpha[n]} = j\alpha[n]$, we can rewrite $s(t)$ as:

$$s(t) \approx \sum_{n=1}^{\infty} a_0[n-1] j\alpha[n] h_0(t - nT) \tag{3.6}$$

where, $a_0[n-1] \in \{\pm 1, \pm j\}$, or

$$s(t) \approx \sum_{n=1}^{\infty} j^n a[n-1]\alpha[n] h_0(t - nT) \tag{3.7}$$

where, $a[n] \in \{\pm 1\}$. A block diagram of an one-pulse(1P) approximation of GMSK modulator is given in Figure 3.2.

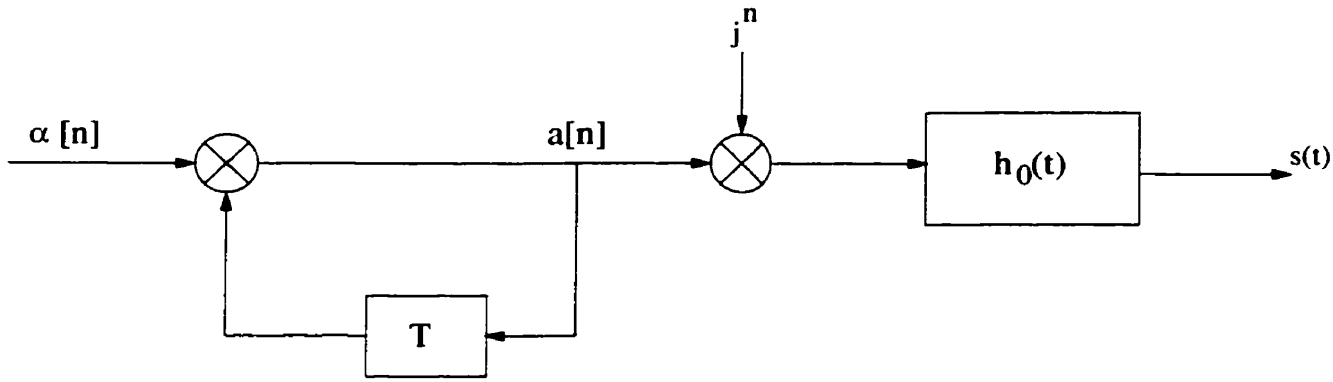


Figure 3.2: The Laurent modulator

### 3.1.1 Approximating GMSK as Binary Differential PSK

The approximated GMSK modulator consists of a differential encoder, an I/Q mapper(which can also be seen as a 90 degree phase rotation), and a transmitter filter, $h_0$. In this section, we will show that with a simple derotation at the receiver, we can approximate the Laurent-based GMSK transmission system by a Binary Differential PSK(BDPSK) transmission system. Figure 3.3 shows a block diagram of the discrete-time 1P approximated GMSK transmission model. The received signal, sampled at times kT at the output of the receiver input filter can be written as:

$$r[k] = \sum_{n=0}^{L_h-1} h_n a[k-n] j^{k-n} + n[k] \tag{3.8}$$

where $\alpha[k]$ is the antipodal input symbol and $a[k] = \alpha[k]a[k-1]$. $h_n, 0 \leq n \leq L_h - 1$, are the coefficients of the combined discrete-time impulse response of the transmit filter, channel, and receiver input filter;its length is denoted by $L_h$. $n[k]$ represents complex additive Gaussian noise with a one-sided power spectral density of $N_0$. First we recognize that:

$$r[k] = \sum_{n=0}^{L_h-1} h_n a[k-n] j^{k-n} + n[k] = j^k \sum_{n=0}^{L_h-1} h_n a[k-n] j^{-n} + n[k] \tag{3.9}$$

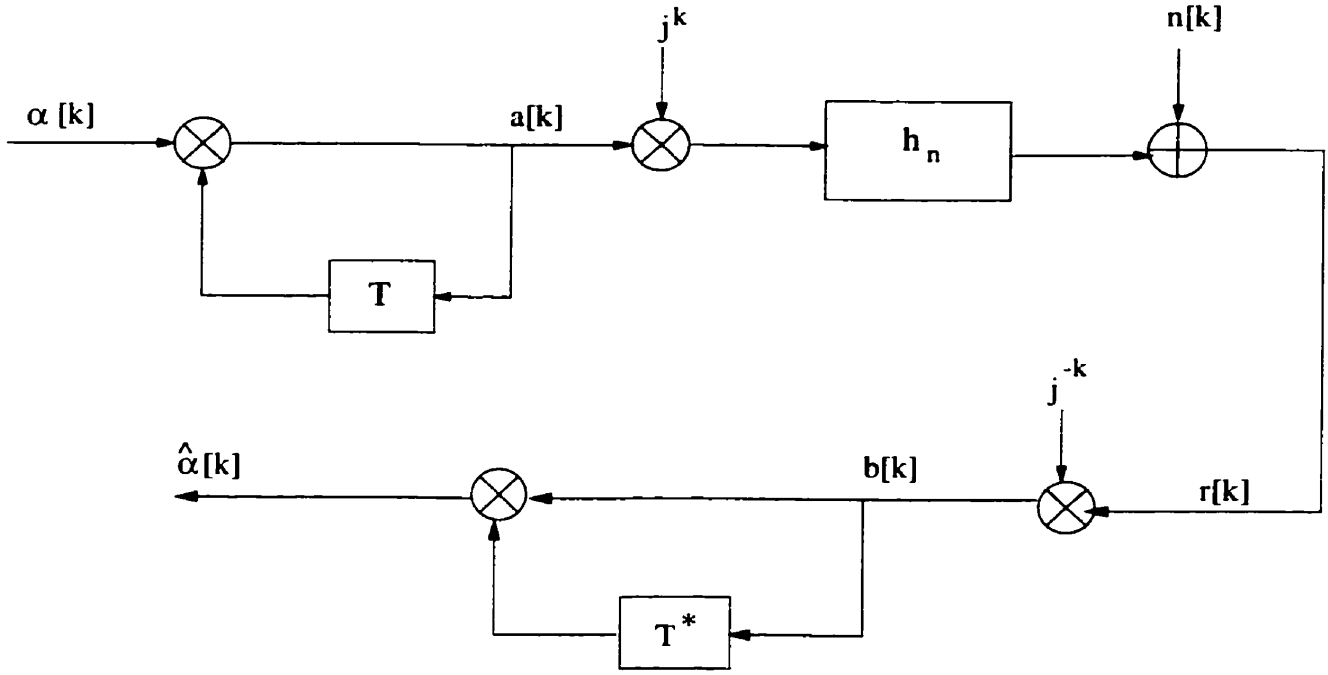


Figure 3.3: Block diagram of the discrete-time Laurent-based transmission model

By applying derotation $j^{-k}$, we have:

$$b[k] = r[k]j^{-k} = \sum_{n=0}^{L_h-1} [h_n j^{-n}]a[k-n] + n[k]j^{-k} \tag{3.10}$$

Note that multiplying $n[k]$ with $j^{-k}$ doesn't change the statistical property of $n[k]$. Let $g_n = h_n j^{-n}$, we now have

$$b[k] = \sum_{n=0}^{L_g-1} g_n a[k-n] + n[k] \tag{3.11}$$

$b[k]$ can then be decoded using a feedforward decoder to obtain the input bits $\hat{\alpha}[k]$. A block diagram of BDPSK approximation of GMSK is shown in Figure 3.4. We have shown that the 1P Laurent approximation of GMSK transmission system can be seen as a BDPSK transmission system.

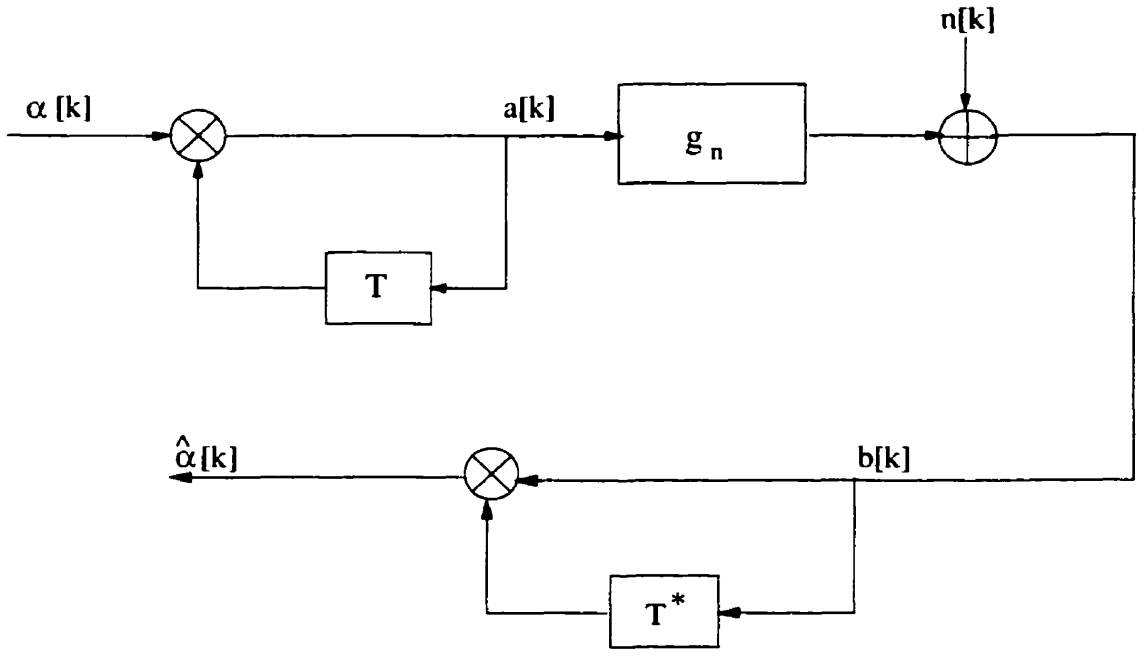


Figure 3.4: Block diagram of the discrete-time BPSK-based transmission model

## 3.2 Detecting GMSK with A Coherent Adaptive DFE

If synchronization is possible and inexpensive, it is well known that a coherent detection scheme outperforms a noncoherent detection scheme. Therefore, we will first implement a coherent PSK-Based GMSK receiver. The performance of the coherent scheme will be used as a benchmark for the noncoherent scheme. For simplicity, we will derive the receiver using the BDPSK transmission model shown in Figure 3.4. In a coherent AWGN channel, matched filtering is an optimal front-end for the receiver because it maximizes the SNR and provides sufficient statistics for detection. Therefore, the receiver filter is matched to the main Laurent pulse. However, this matched filtering introduces additional ISI. This is clearly shown in Figure 3.5 and Figure 3.6. Figure 3.5 shows the eye diagrams for the signal(I and Q ) at the input of the matched filter and Figure 3.6 shows the eye diagrams for the signal at the output

of the matched filter(assumed noiseless). As a result, coherent adaptive DFE must

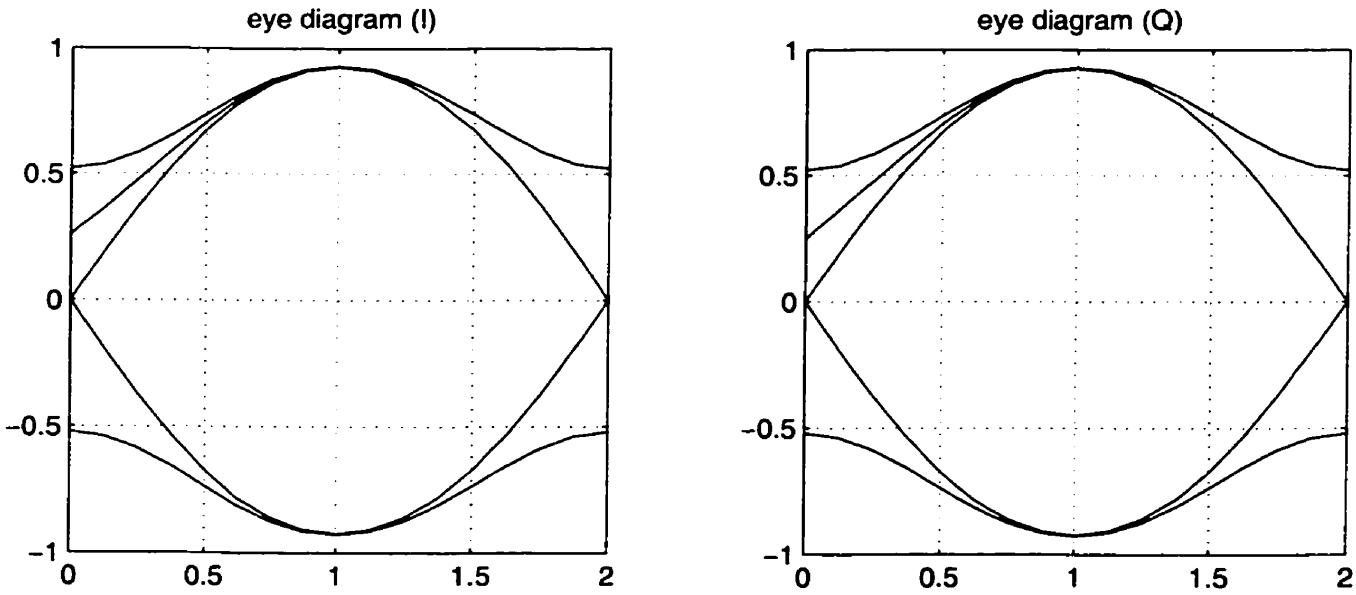


Figure 3.5: Eye diagram of signals before the matched filter

be used to mitigate the effects of ISI. Figure 3.7 shows a block diagram of the coherent receiver. In the Figure, $r(t) = s(t) + n(t)$, where $s(t)$ is the transmitted signal, $n(t)$ represents complex additive Gaussian noise with a one-sided power spectral density of $N_0$ and $h$ is the receiver filter. After sampling, the bits are treated as differentially encoded BPSK bits and fed into a coherent adaptive DFE(4,2). The DFE has 4 coefficients in the feedforward filter and 2 coefficients in the feedback filter. It is found that there is no appreciable improvements in performance when longer filters are used. For filter adaptation, conventional RLS algorithm is used with $w = 0.98$. A data block containing a training sequence of 200 bits is used for the equalizer to learn about the channel characteristics. The actual data sequence is 20000 bits long. Here, since we are not trying to model any specific standard, the data block length is chosen arbitrarily. Since we are dealing with a static channel, after training, the DFE adaptation is switched off. The DFE structure and the adaptation algorithm of coherent adaptive DFE were introduced in Chapter 2 and are well explained in [2],

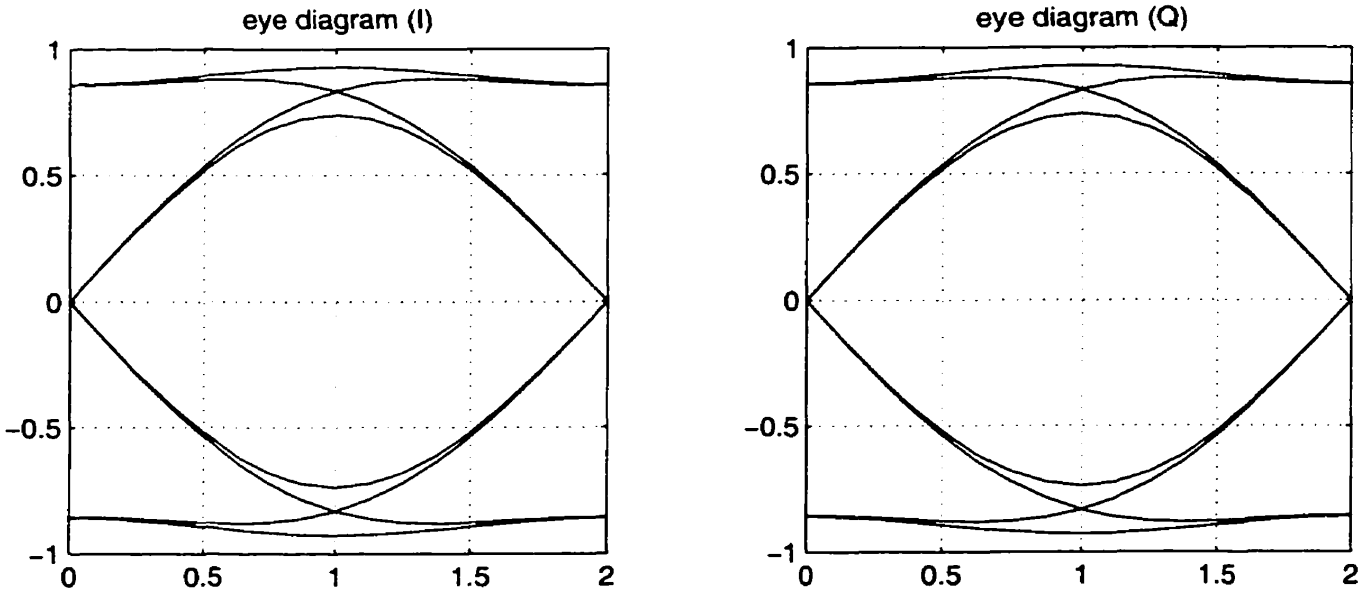


Figure 3.6: Eye diagram of signals after the matched filter

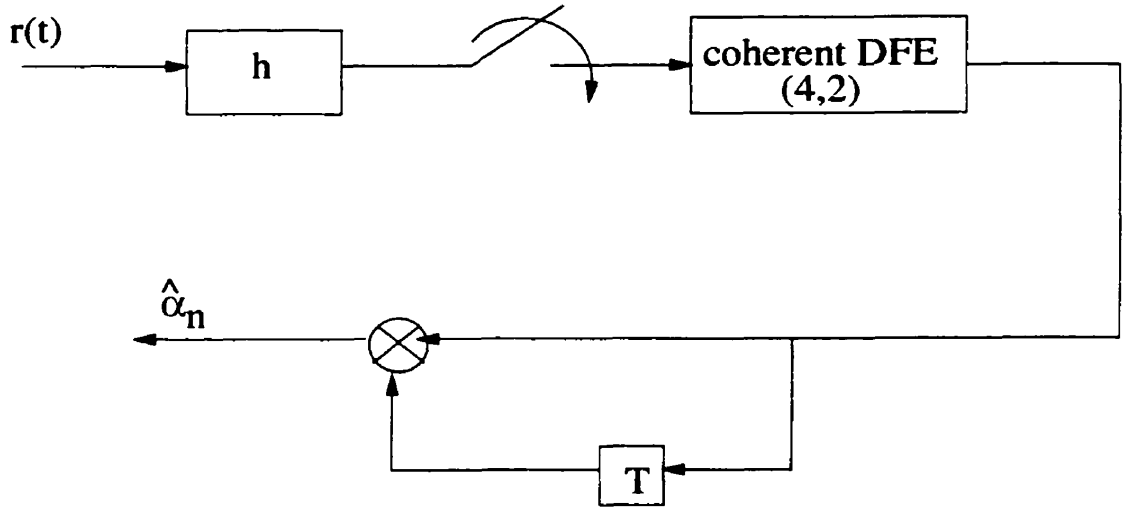


Figure 3.7: PSK-based coherent receiver

we will not discuss it further here. In this thesis, the signal to noise ratio(SNR) is defined as $E_b/N_0$.

### 3.2.1 Coherent GMSK Receiver Performance

In order to find the performance loss due to the 1P approximation, the PSK-based coherent receiver shown in Figure 3.7 will be used to receive actual GMSK signals(generated by Figure 2.1) and approximated GMSK signals (generated by Figure 3.2). Since the receiver is designed according to the 1P approximation of GMSK, we expect the performance of the receiver receiving actual GMSK signals to be worse than the performance of the receiver receiving the approximated GMSK signals. Furthermore, since the 1P approximation contains most of the GMSK energy, we expect the performance difference to be small. However, computer simulation results contradict our expectation. From Figure 3.8, we see that the receiver receiving the actual GMSK signals performs much worse than receiving the approximated GMSK signals. Further analysis shows that when receiving real GMSK signals, the DFE filter taps failed to converge. This indicates that the ISI may be time-varying.

### 3.2.2 Simulating GMSK

In section 2.1.1, we mentioned that g(t), the GMSK frequency pulse is normally truncated to LT. For GMSK with BT=0.3, L is chosen to be 3. When simulating the GMSK modulator, we used the truncated g(t). Since the phase function q(t) is the integral of g(t), the truncation of g(t) causes instability of GMSK phase. This instability in turn causes the instability of DFE algorithm. To illustrate this, assume that the GMSK modulator presented in Figure 2.1 is used to modulate an all 1 input data block. Ideally, the phase of the modulated signals should be a linear continuously increasing function. Figure 3.9 shows the plot of such a function(phase is normally represented between $\pi$ and $-\pi$). When truncation is applied to g(t), it creates discontinuity in the phase function. Figure 3.10 shows that the truncation loss causes

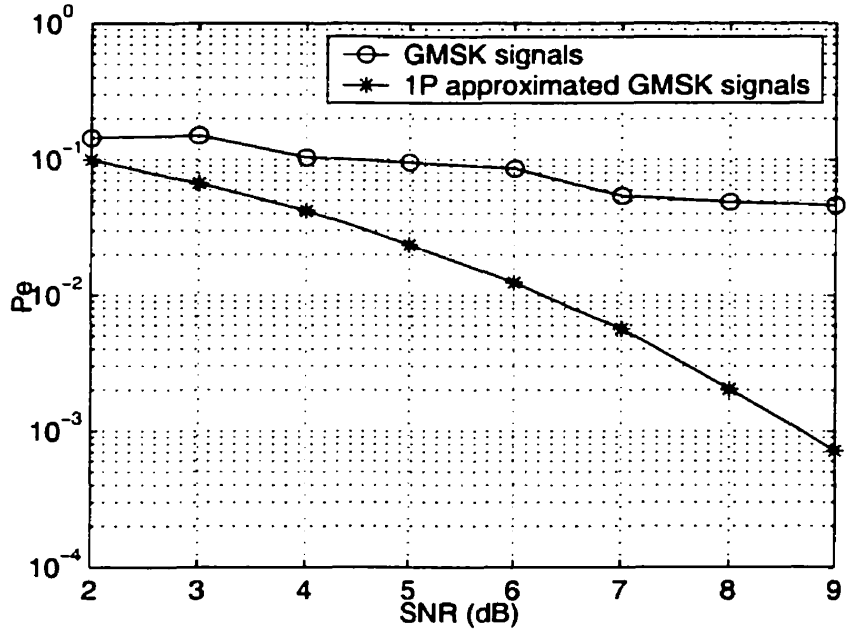


Figure 3.8: BER performance of the PSK-based receiver receiving 1P approximated GMSK signals and GMSK signals in an AWGN channel

the phase of GMSK signal to fluctuate. This fluctuation in turn caused the ISI to be time-varying. Therefore, the initial training of DFE did not provide convergence. To solve this problem, a truncation of L=7 is used in the simulation of GMSK modulator. Note that to obtain a Laurent representation, L=3 is still sufficient. Using the improved GMSK modulator, Figure 3.11 shows that the performance of the receiver receiving the actual GMSK signals is very close to the approximated GMSK signals. Therefore, GMSK can be well approximated as BDPSK in a coherent system.

### 3.2.3 Sensitivity to Frequency Offset

One of the major problem of coherent detection scheme is its sensitivity to frequency offsets. However, a practical wireless channel sometimes introduces phase drift, which would cause frequency offset. This can be represented by $r(t)e^{jt\Delta f}$, where $r(t)$ is the received signal. Coherent adaptive DFE can not cope with this impairment even when

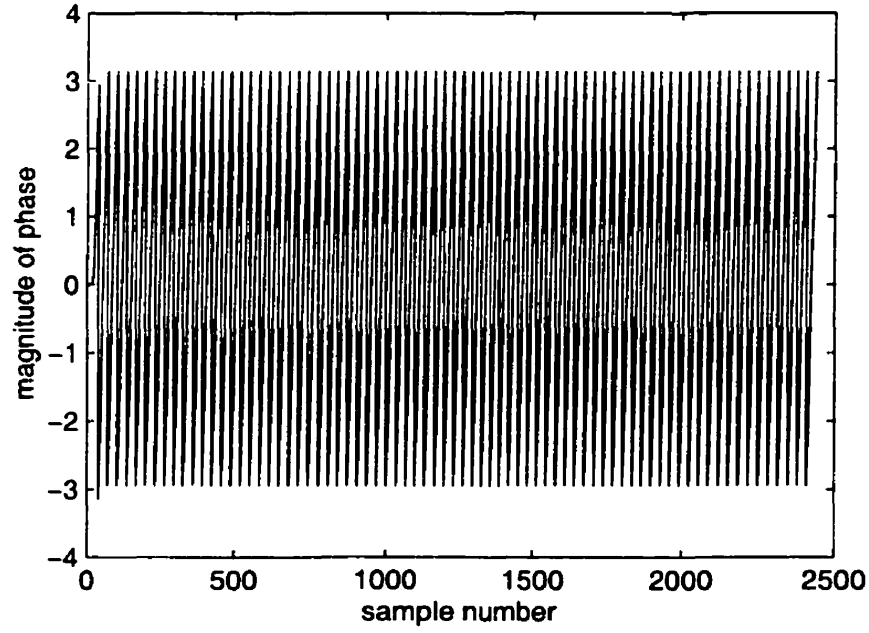


Figure 3.9: Ideal phase plot of GMSK signals with all 1s as input

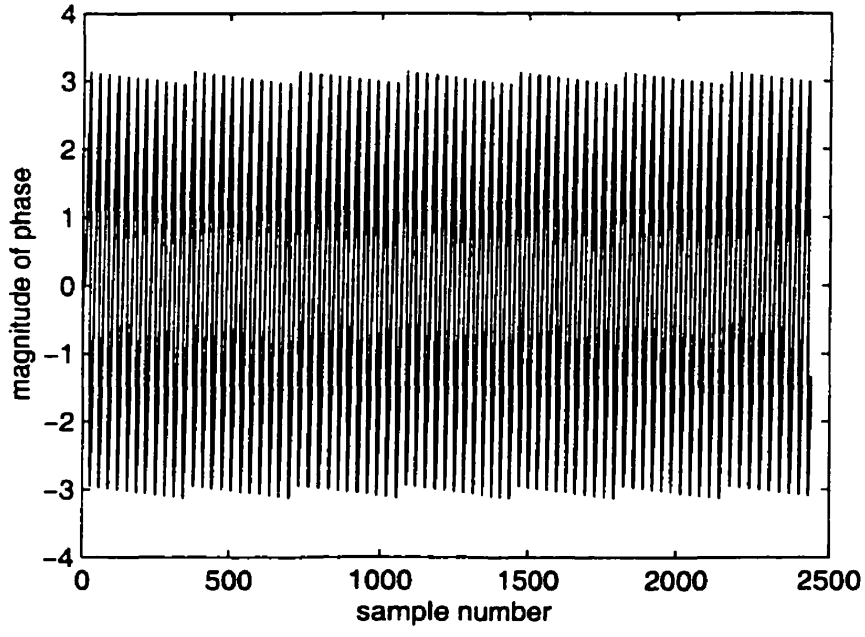


Figure 3.10: Phase plot of GMSK signals with all 1s as input and L=3

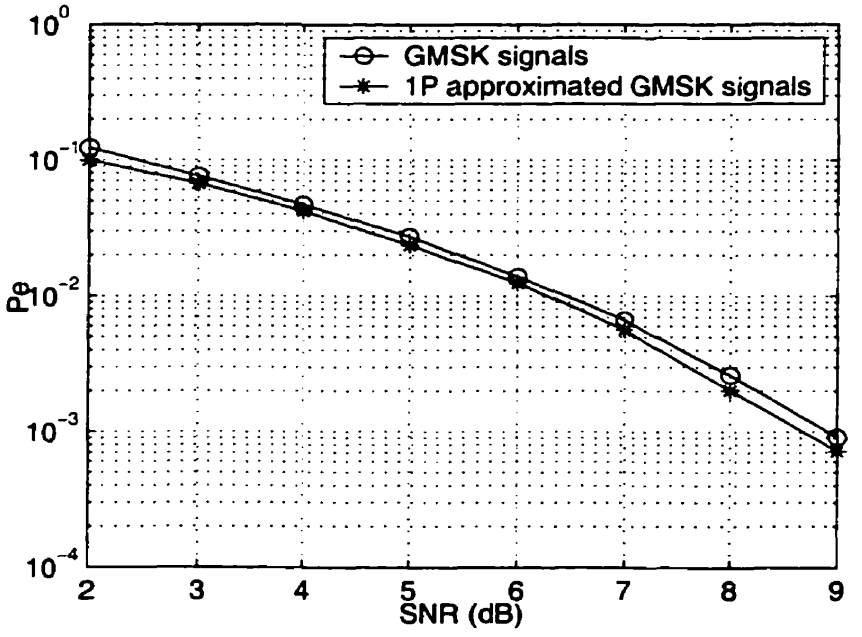


Figure 3.11: Performance of the PSK-based receiver receiving 1P approximated GMSK signals and GMSK signals

running in decision directed mode. In Figure 3.12, the performance of the coherent receiver receiving GMSK signals is evaluated for a constant frequency offset $\Delta f$ at $SNR = 8dB$. We see that coherent adaptive DFE fails to equalize even for very small frequency offsets. This shows that the conventional RLS algorithm is unable to track the phase variations[2].

## 3.3 Differential Detection of GMSK signals with Adaptive NDFE

We have seen that coherent equalizers are not capable of compensating for the time-varying phase. In addition, in many applications, it is not possible to perform coherent detection due to the inability of the receiver to produce carrier phase estimates. Therefore, differential detection, which obviates the need for implementing the carrier

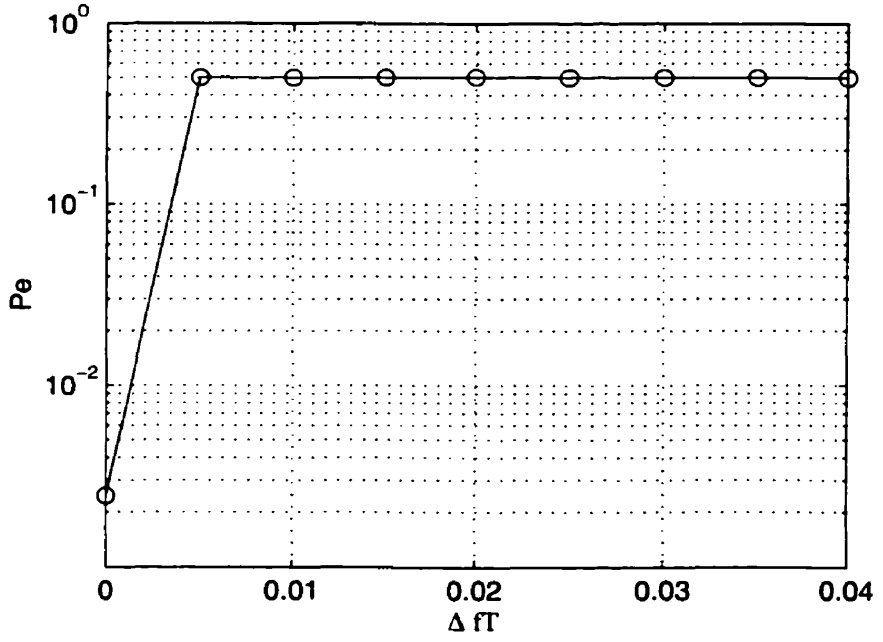


Figure 3.12: Probability of error versus $\Delta fT$ for coherent detection

synchronization function, is an attractive alternative to coherent detection. In chapter 2, we briefly introduced Schober's NDFE scheme. In this section, we will discuss detecting GMSK signals with Schober's adaptive NDFE.

### 3.3.1 Schober's Adaptive NDFE

Schober's adaptive NDFE scheme is proposed for M-ary differential PSK signals. First, we will discuss in more detail the NDFE algorithm. Figure 3.13 shows a block diagram of a complex baseband discrete-time M-ary differential PSK transmission model used in deriving the algorithm[29]. The information symbols $a[k] \in \{e^{j2\pi\nu/M} \mid \nu \in \{0, 1, ..., M-1\}\}$, which are independent and identically distributed random variables, are differentially encoded into the symbols $b[k]$ as follows:

$$b[k] = a[k]b[k-1], \quad k = 1, 2, ...$$

where $b[0] = 1$. The transmitter filter has a real impulse response corresponding to square-root raised cosine spectrum. The receiver filter is matched to the transmitter

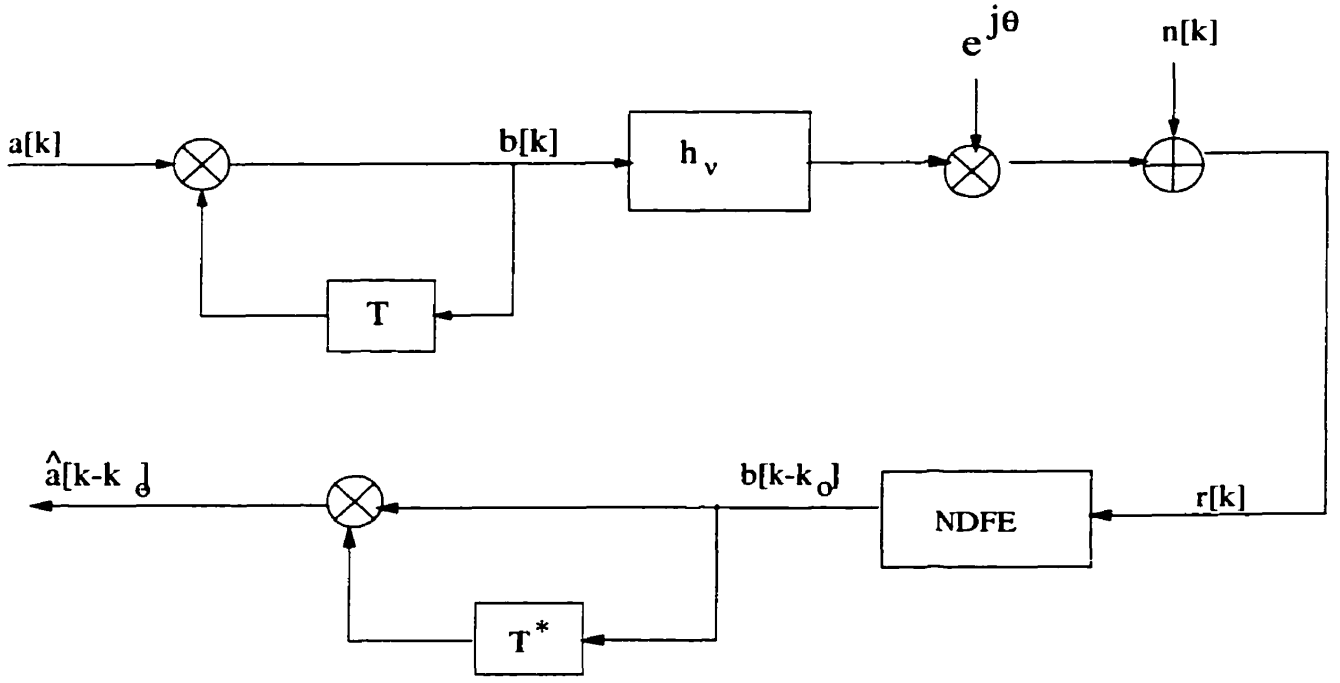


Figure 3.13: Block diagram of the discrete-time transmission model for MPSK signals

filter. The received signal, sampled at time kT at the output of the receiver input filter can be written as

$$r[k] = e^{j\theta} \sum_{\nu=0}^{L_h-1} h_\nu b[k-\nu] + n[k] \tag{3.12}$$

where $\theta$ denotes an unknown, constant, uniformly distributed phase introduced by the channel. $h_\nu, 0 \leq n \leq L_h - 1$, are the coefficients of the combined discrete-time impulse response of the transmit filter, channel, and receiver input filter; its length is denoted by $L_h$. $n[k]$ represents complex additive Gaussian noise with a one-sided power spectral density of $N_0$. After passing through the noncoherent DFE, the estimated MPSK symbols, $\hat{b}[k-k_0]$ are decoded back to $\hat{a}[k-k_0]$

$$\hat{a}[k] = \hat{b}[k-k_0]\hat{b}^*[k-k_0-1] \tag{3.13}$$

where $k_0$ is a decision delay introduced by the NDFE.

Unlike the NDFE schemes discussed in chapter 2, the proposed NDFE is placed before the differential decoder. The structure of the NDFE is shown in Figure 3.14.

In the Figure, $r_{DFE}[k]$ is the output of the NDFE feedforward(FF) filter, $\hat{y}_{DFE}[k]$ is

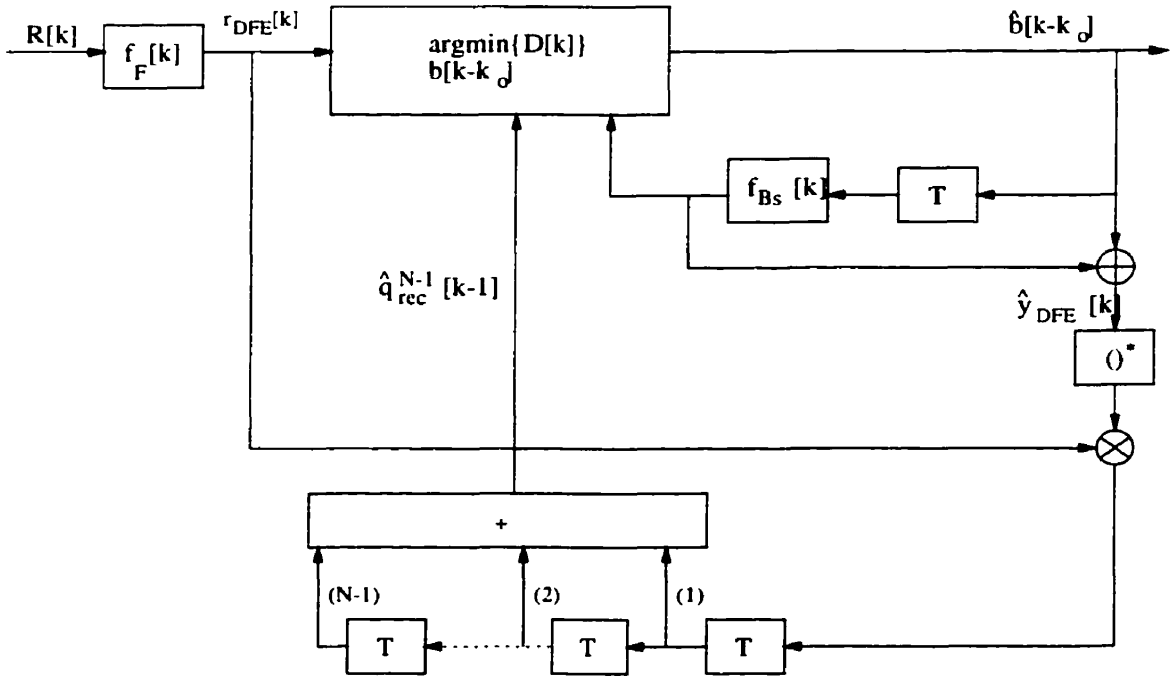


Figure 3.14: Block diagram of Schober's NDFE structure[29]

the output of the NDFE feedback(FB) filter. The FF filter coefficient vector $f_F[k]$ with length $L_F$, the FB filter coefficient vector $f_B[k]$ with length $L_B$ and the received signal samples vector $R[k]$ with length $L_F$ are defined as:

$$f_F[k] \triangleq [f_{F,0}[k]\ f_{F,1}[k]\ \ldots\ f_{F,(L_F-1)}[k]]^H$$

$$R[k] \triangleq [r[k]\ r[k-1]\ \ldots\ r[k-L_F+1]]^T$$

$$f_B[k] \triangleq [f_{B,0}[k]\ f_{B,1}[k]\ \ldots\ f_{B,(L_B-1)}[k]]^H$$

Since FF and FB filters introduce an additional degree of design freedom, the constrain $f_{B,0}[k] \equiv 1$ is used. Thus

$$f_B[k] \triangleq [1\ f_{Bs}[k]]$$

From Appendix A, we see that the NDFE might be interpreted as a noncoherent reduced state MLSE with only one state. The resulting DFE decision rule is given as

[29]:

$$\hat{b}[k-k_0] = argmin \underbrace{\{D[k]\}}_{b[k-k_0]} \tag{3.14}$$

where

$$D[k] \triangleq \mid b[k-k_0] + f_{Bs}^H[k]\hat{c}[k-k_0-1] \mid^2 \tag{3.15}$$

$$-2 \mid r_{DFE}[k](b[k-k_0] + f_{Bs}^H[k]\hat{c}[k-k_0-1])^* \tag{3.16}$$

$$+\hat{q}_{nrec}^{N-1}[k-1] \mid \tag{3.17}$$

$b[k-k_0]$ is the decision,

$$\hat{q}_{nrec}^{N-1}[k-1] \triangleq \sum_{\nu=k-N+1}^{k-1} r_{DFE}[\nu]\hat{y}_{DFE}^*[\nu] \tag{3.18}$$

and

$$\hat{c}[k-k_0-1] \triangleq [\hat{b}[k-k_0-1]\ \hat{b}[k-k_0-2]\ ...\ \hat{b}[k-k0-L_B+1]]^T$$

Note that the decision rule does not depend on the channel phase $\theta$ which is mandatory for a noncoherent receiver. As a result, differential encoding is needed since the absolute phase of the estimated symbol sequence $\hat{b}[k]$ may differ from the absolute phase of the transmitted symbol sequence $b[k]$. The phase of $\hat{q}_{nrec}^{N-1}[k-1]$ is interpreted as an estimation of the phase difference between $r_{DFE}[k]$ and $\hat{y}_{DFE}[k]$. Thus, as N increases, the accuracy of the estimation improves. However, increasing N also increases the required number of computations. Therefore, instead of the summation form, a recursive method can be used to estimate the phase difference:

$$\hat{q}_{rec}[k-1] \triangleq \beta\hat{q}_{rec}[k-2] + r_{DFE}[k-1]\hat{y}_{DFE}^*[k-1] \tag{3.19}$$

where $\beta$, $0 \leq \beta \leq 1$, is a forgetting factor. Note that $\hat{q}_{nrec}^{N-1}[k-1]$ and $\hat{q}_{rec}[k-1]$ are identical as $N \to \infty$ and $\beta \to 1$.

Since this is a noncoherent scheme, there is no simple filter design criterion based on minimization of an error variance. Therefore, $E\{D[k]\}$ is used as the cost function

for calculation of the FF and FB filters. The filter settings for $f_F[k]$ and $f_B[k]$ can be calculated from

$$\frac{\partial}{\partial f_X^*[k]} E\{D[k]\} = 0_{S_X}, \quad X = F, B \tag{3.20}$$

where $0_{S_X}$ denotes the all zeros vector with $S_X$ rows. For finite N, it is very difficult to find the solution analytically. The authors derived the modified LMS and RLS algorithms to find the desired filter settings[29]. For illustration purpose, the modified LMS algorithm is given below:

The FF filter coefficient vector is updated according to

$$f_F[k+1] = f_F[k] + \delta e_F^* R[k] \tag{3.21}$$

with

$$e_F[k] = \frac{q_{rec}[k]}{\mid q_{rec}[k] \mid} \hat{y}_{DFE}[k] - r_{DFE}[k] \tag{3.22}$$

where $\delta$ is the adaptation step size. Similarly, the feedback filter coefficients can be updated as

$$f_B[k+1] = f_B[k] + \delta e_B^* c[k] \tag{3.23}$$

with

$$e_B[k] = \frac{q_{rec}^*[k]}{\mid q_{rec}[k] \mid} r_{DFE}[k] - \hat{y}_{DFE}[k] \tag{3.24}$$

To calculate $e_F[k]$ and $e_B[k]$, knowledge of the transmitted symbol sequence $b[k]$ is necessary. Therefore, a training sequence is needed for adaptation of the FF and FB filter coefficients. The modified LMS algorithm is very similar to the conventional LMS. When compared to conventional LMS algorithm, the only difference is the factor $\frac{q_{rec}[k]}{|q_{rec}[k]|}$ and $\frac{q_{rec}^*[k]}{|q_{rec}[k]|}$ for calculation of $e_F[k]$ and $e_B[k]$. Furthermore, at time $k = 0$, all FF and FB filter coefficients are initialized with zeros. At $k = 1$, $\frac{q_{rec}[k]}{|q_{rec}[k]|} = 1$ is used. $k_0$, the delay introduced by DFE,can be determined by using $k_0 = L_F + L_h - 1 - L_B$.

It is shown both analytically and through simulation that as $\beta$ increases, the performance of the proposed NDFE increases[29]. As $\beta \rightarrow 1$, the performance of the NDFE is the same as coherent DFE. To illustrate this, we will compare the

performance of a coherent DFE(4,2) with the NDFE(4,2) by using the proposed PSK-based receiver receiving 1P approximated GMSK signals. Figure 3.15 shows that at $\beta = 0.9$, there is only a very small difference. It is shown in last section that the

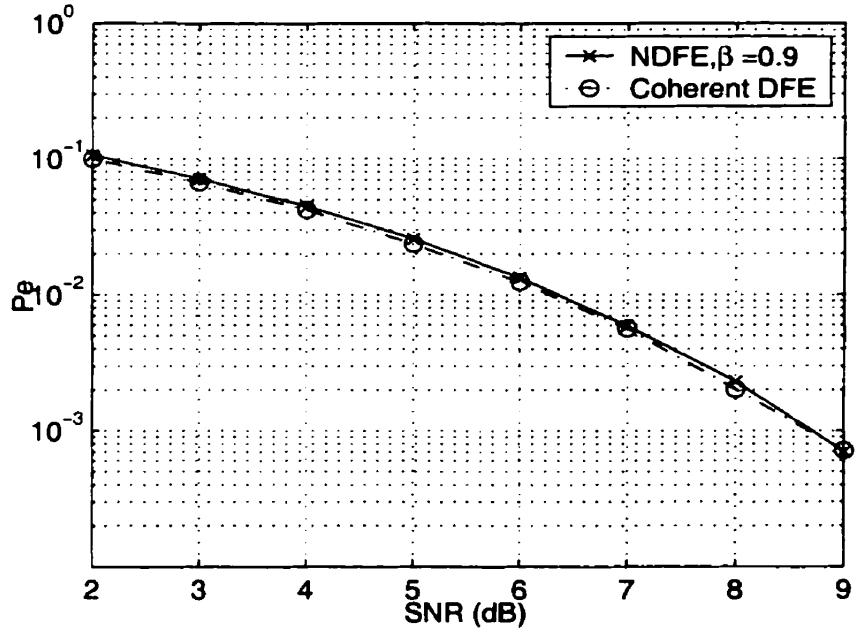


Figure 3.15: BER Performance of the PSK-based receiver receiving 1P approximated GMSK signals with coherent DFE versus NDFE at $\beta = 0.9$

coherent DFE fails to function when a frequency offset is present, and the NDFE can track this frequency offset by decreasing $\beta$. It is shown through simulation that as $\beta$ decreases, the frequency sensitivity decreases as well[29]. This will be demonstrated later in the chapter. Therefore, for the NDFE, there is a tradeoff between performance and sensitivity to frequency offset.

### 3.3.2 Noncoherent GMSK Receiver Performance

From section 3.1.1, we see that GMSK can be well approximated as BDPSK in coherent system. Therefore, we will apply Schober's DFE algorithm directly to GMSK signals. For the simulations, the modified RLS algorithm(presented in Appendix B

along with its learning curve) with $w = 0.98$, is used for adaptation of NDFE taps. For each data block, the training sequence is 200 bits long and the actual data is 20000 bits long. To have a fair comparison, the NDFE has the same number of FF and FB filter taps as the coherent DFE. Since the outputs of matched filter are sufficient statistics for symbol detection, we will continue to use the matched filter as the receiver front-end filter. Figure 3.16 compares the performance of the proposed noncoherent receiver receiving the 1P approximated GMSK signals and receiving the actual GMSK signals with L=7. The figure shows that the performance of the re-

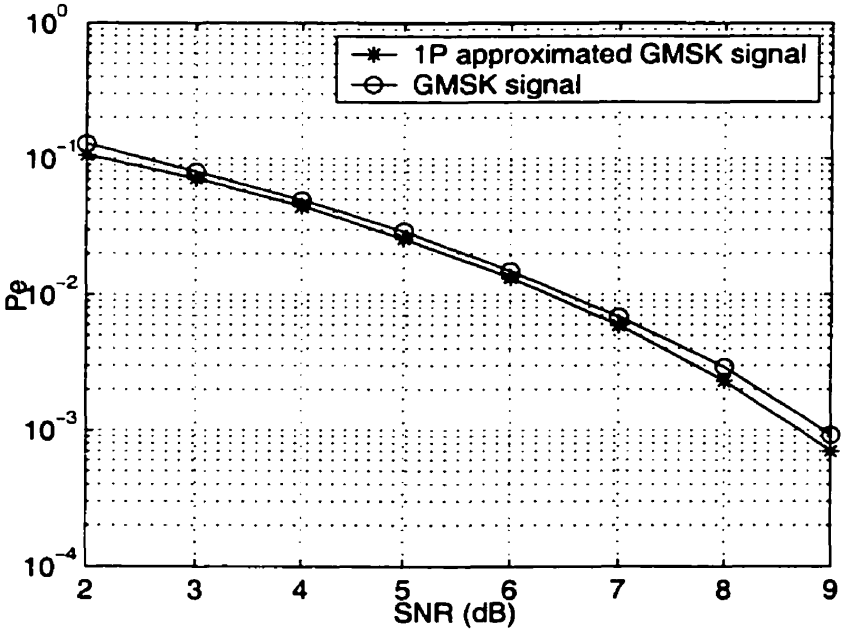


Figure 3.16: BER Performance of the receiver with NDFE receiving GMSK signal and 1P approximated GMSK signal at $\beta = 0.9$

ceiver receiving the actual GMSK signals is very close to that of the approximated GMSK signals. Therefore, we have shown that GMSK can be well approximated as BDPSK in noncoherent system. In addition, the performance of the noncoherent GMSK receiver is compared to the performance of the optimum coherent GMSK coherent receiver. For the simulation, actual GMSK signals are used. As can be seen in Figure 3.17, the noncoherent receiver suffers only about 1.5 dB loss BT=0.3.

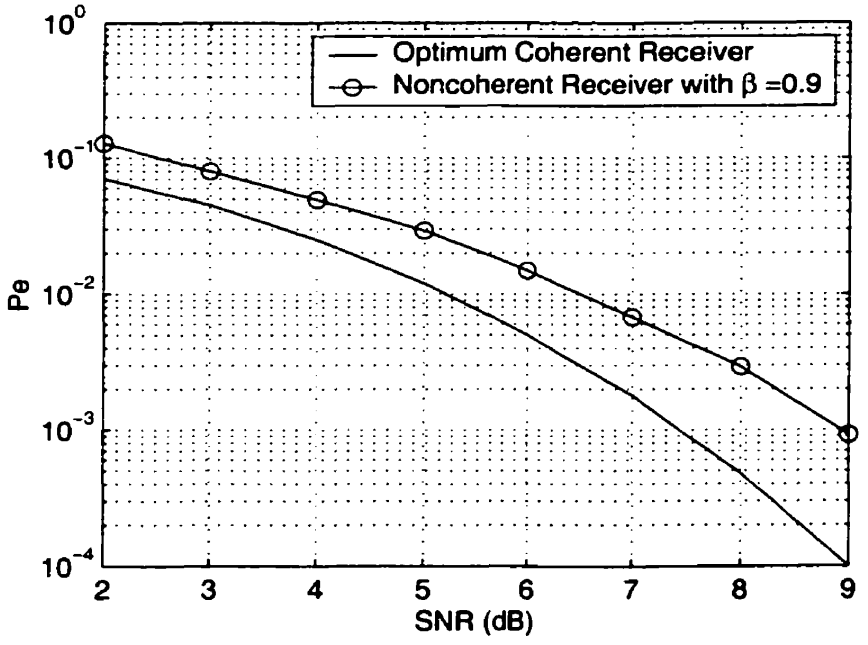


Figure 3.17: BER Performance of optimum coherent receiver versus proposed noncoherent receiver at $\beta = 0.9$

### 3.3.3 Sensitivity to Frequency Offset

In this section, we will investigate the sensitivity of the proposed noncoherent GMSK receiver to frequency offset. From here on, actual GMSK signals are used for all simulations and the performance of the coherent GMSK receiver is included when appropriate. Figure 3.18 compares the performance of the receivers with $\beta = 0.9$, $\beta = 0.6$ and $\beta = 0.4$. The plot verifies that as $\beta$ increases to 1, the performance of the noncoherent receiver approaches the performance of the coherent receiver. The noncoherent receivers are then compared for their ability to handle frequency offset. For the simulation, a constant frequency offset $\Delta f$ at $SNR = 8dB$ is introduced. Figure 3.19 show that though $\beta = 0.4$ performs the worst when no frequency offset is present, it is the best when severe frequency offset is present. Hence we have shown that there is a tradeoff between the receiver's sensitivity to frequency offset and its performance. To explain this tradeoff, we have to take a close look at the

NDFE structure. The phase of $q_{rec}[k-1]$ might be interpreted as the estimate for the phase difference between $r_{DFE}[k]$ and $\hat{y}_{DFE}[k]$. If we assume the phase difference is a constant value(no frequency offset), as $\beta \rightarrow 1$, the accuracy of this estimate increases, which improves the performance. However, if the phase difference is time variant value(frequency offset is present), as $\beta \rightarrow 1$, the phase of $q_{rec}[k-1]$ can not be used to track the changes in the phase difference. Smaller $\beta$ value is more robust for the changes, which results in better performance.

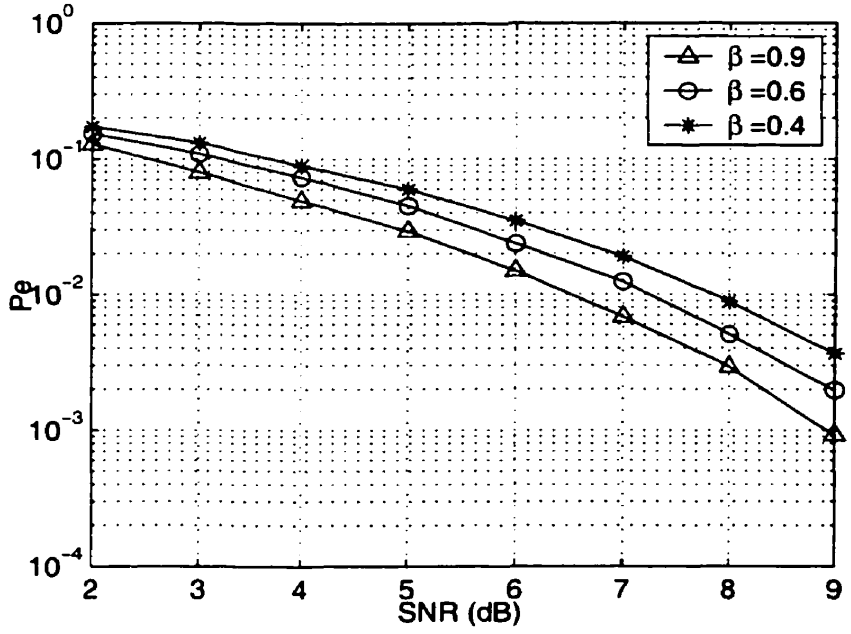


Figure 3.18: BER Performance of the noncoherent receiver with different $\beta$

### 3.3.4 The Role of BT

So far, we only considered GMSK with $BT = 0.3$. This section investigates the performance of the noncoherent receiver for different BT values. From chapter 2, we have seen that by increasing BT, the duration of GMSK phase function is reduced. This reduction in duration translates to reduction in duration of Laurent pulses L, thus, less ISI. Therefore, it is expected that as BT increases, the BER performance of

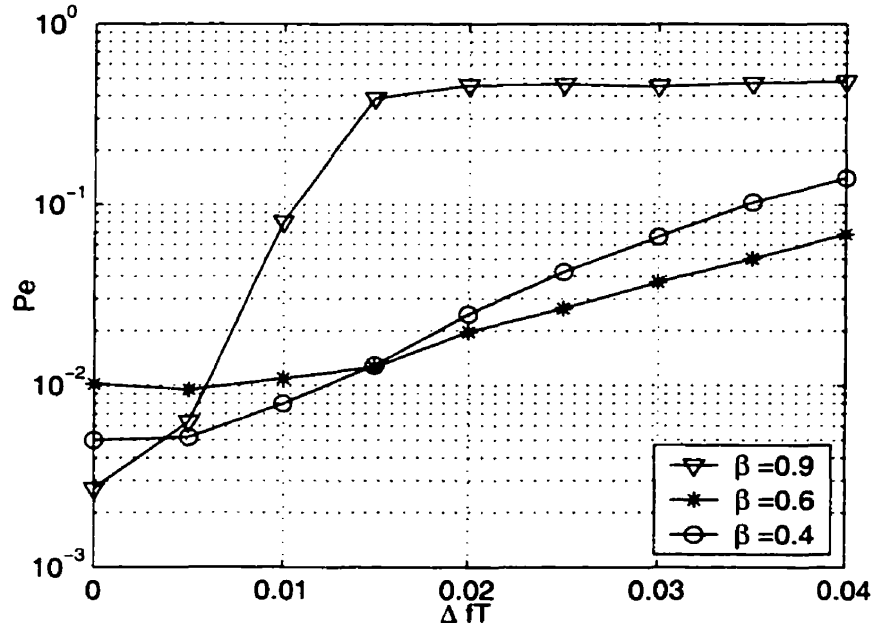


Figure 3.19: Probability of error versus $\Delta fT$ for the noncoherent receiver with different $\beta$

the noncoherent receiver will increase. This is verified in Figure 3.20. In the figure, the performance of noncoherent detection of DBPSK and MSK are also plotted for reference. The probability of error for DBPSK and MSK in AWGN channel are given as [2]:

$$Pe = \frac{1}{2}e^{-E_b/N_0} \tag{3.25}$$

However, as BT increases, the spectral efficiency of GMSK decreases. Figure 3.21 shows the power spectrum of the GMSK signal versus the normalized frequency with BT as a parameter. This figure is generated by using Welch's method for spectrum estimation.[37] Therefore, there is a tradeoff between performance and spectrum efficiency for the proposed receiver.

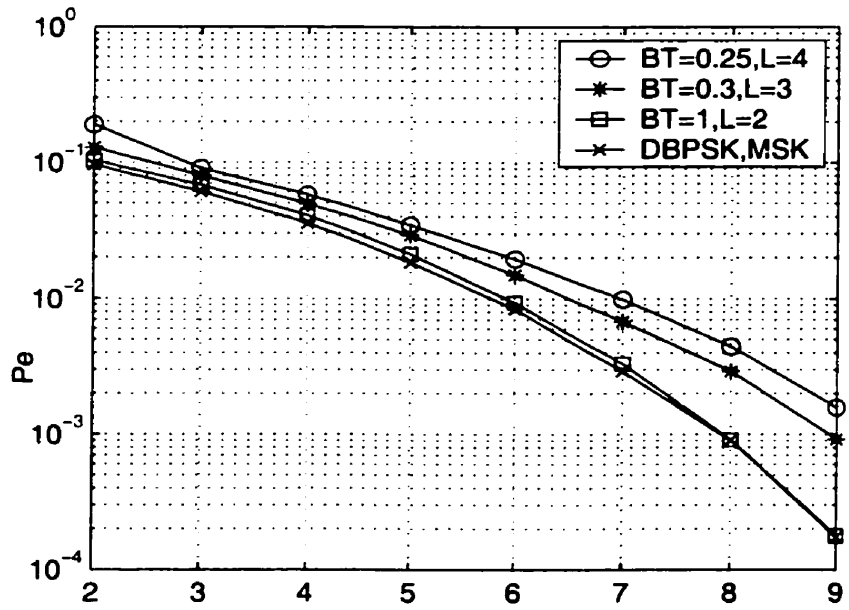


Figure 3.20: BER Performance of the noncoherent receiver with different BT and L

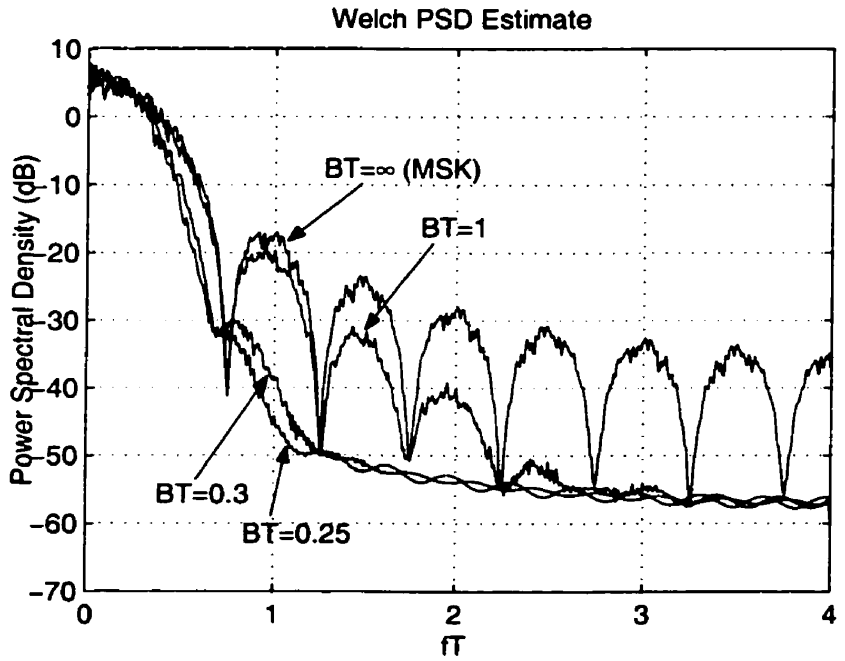


Figure 3.21: Power spectra of GMSK

### 3.3.5 Fractionally Spaced NDFE

For linear modulation, the optimum receiver filter is the cascade of a filter matched to the actual channel, with a transversal T-spaced equalizer[2]. By reducing the sampling phase sensitivity relative to T-spaced equalizer, the fractionally spaced equalizer can synthesize the best combination of the matched filter and a T-spaced equalizer for maximum likelihood detection. This advantage is not as important for GMSK modulation since there is no single receiver filter that can match exactly to the transmitter filter. In addition, the difference between the best and worst timing epochs is much smaller for the DFE than for a LE[21]. Therefore, for GMSK modulation, fractionally spaced NDFE has no performance advantage over T-spaced NDFE. This is verified by computer simulation by using the proposed NDFE, for $BT = 0.3$, $\beta = 0.9$. The feedforward tap spacing of the fractionally spaced NDFE is $\frac{T}{2}$. To cover the same channel span as T-spaced NDFE, fractionally spaced NDFE requires twice as many FF filter taps as the T-spaced NDFE. The simulation result is shown in Figure 3.22. The figure shows no performance improvement by using fractionally spaced NDFE. Similar result is also reported in [22] for coherent detection of GMSK signals.

### 3.3.6 Performance Versus Other Noncoherent GMSK Receivers

It was shown that at $\beta = 0.9$, the proposed noncoherent GMSK receiver performs very close to a corresponding coherent receiver. In addition, we will compare the proposed receiver at $\beta = 0.9$ to three other noncoherent receivers presented in [38],[15] and [39]. In [38], Korn proposed a noncoherent GMSK receiver by employing limiter-discriminator and 2-bit decision feedback. In [15], Yongacoglu et al. proposed a noncoherent GMSK receiver by combining 2 and 3-bit differential detection and decision feedback. In [39], Colavolpe et al. proposed a noncoherent GMSK receiver based on noncoherent sequence detection using the Viterbi algorithm with 32 states. It is

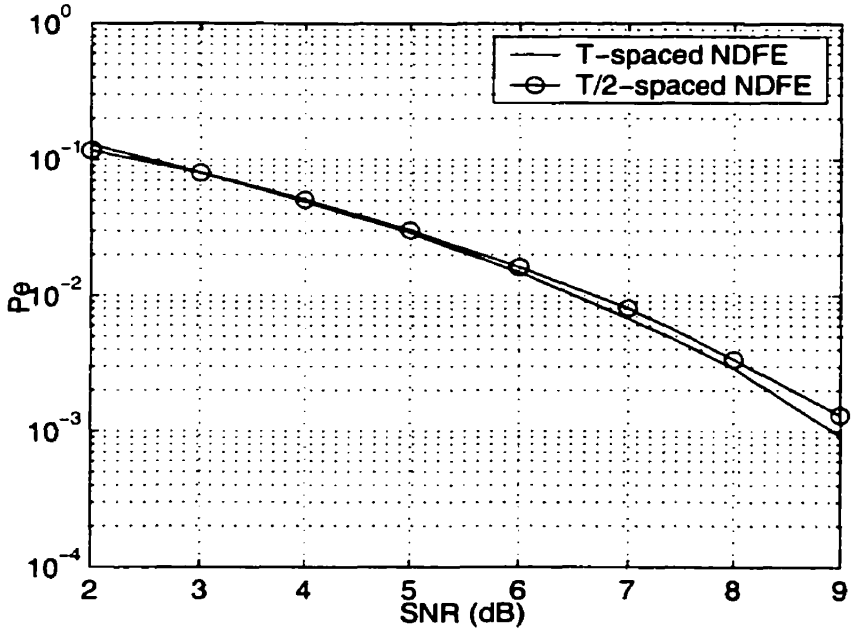


Figure 3.22: BER Performance of the receiver with T-spaced NDFE and T/2-spaced NDFE

found that the receiver proposed by us is slightly more computationally complex than the receivers proposed by Korn and Yongacoglu. However, the receiver proposed by Colavolpe is much more complex than the receiver proposed by us. Table 3.1 compares the BER performances with $BT = 0.25$ under AWGN channel. From the table, we see that with slightly higher computational complexity, the receiver proposed by us outperforms the receivers proposed by Korn and Yongacoglu. However, the receiver proposed by Colavolpe performs better than the receiver proposed by us at the price of a much higher computational complexity. Thus, we conclude that the receiver proposed by us is a high performance noncoherent receiver when compared to other known noncoherent GMSK receivers.

Table 3.1: BER performance comparison of various noncoherent receiver at $BT = 0.25$ under AWGN channel

| | SNR (dB) | | | |
|---|---|---|---|---|
| BER | Proposed | Korn[38] | Yongacoglu[15] | Colavolpe[39] |
| $10^{-2}$ | 7 | 9 | 9 | 6.25 |
| $10^{-3}$ | 9.3 | 12.2 | 11 | 8.6 |

# Chapter 4

# Reduced-complexity Noncoherent Receiver in Fading Channels

In the previous chapter, we proposed a noncoherent GMSK receiver. We investigated the performance of the receiver in AWGN channel where the primary source of error is the thermal noise. However, in wireless systems, more errors are caused by fading and multipath effects. Therefore, analyzing the performance of a wireless communication system requires more complex channel models.

This chapter investigates the performance of the proposed noncoherent receiver in fading channels. Section 4.1 investigates the receiver's performance in two static Finite Impulse Response(FIR) channels. The effects of parameters, $\beta$(the NDFE's forgetting factor) and $BT$(GMSK's spreading factor), on the receiver's overall performance will be discussed. Section 4.2 investigates the effects of the same parameters on the overall performance of the receiver under flat Rayleigh fading channel. In addition, the effects of multipath delay spread on the performance of the receiver will be discussed.

## 4.1 Performance Under Static Channels

In a communication system, the overall channel $h(t)$ is defined as the convolution of the transmitter pulse $h_t(t)$, the channel impulse response $h_i(t)$ and the receiver filter $h_r(t)$

$$h(t) = h_t(t) \otimes h_i(t) \otimes h_r(t) \tag{4.1}$$

Using the properties of Fourier transform, (4.1) can be expressed in the frequency domain as:

$$H(f) = H_t(f)H_i(f)H_r(f) \tag{4.2}$$

Since the transmitter and the receiver filters are fixed, the overall channel severity is determined by the channel impulse response. In this section, we will consider two fading channels for $h_i(t)$, channel A: $h_a(t)$ and channel B: $h_b(t)$. They are defined as follows:

$$h_a(t) = 0.3040\delta(t+T) + 0.9029\delta(t) + 0.3040\delta(t-T) \tag{4.3}$$

$$h_b(t) = 0.4079\delta(t+T) + 0.8168\delta(t) + 0.4079\delta(t-T) \tag{4.4}$$

where $\delta(t)$ is the impulse function. The two fading channel models are 3-taps Finite Impulse Response(FIR) models. In the next section, we will discuss their characteristics in detail.

### 4.1.1 Static Channels

Channel A ([0.3040 0.9029 0.3040]) is a is non-null linear phase channel. Figure 4.1 illustrate the impulse response of channel A. Figure 4.2 illustrates the frequency magnitude response of channel A. From Figure 4.2, we observe that the magnitude response has a minimum at $f = \frac{1}{2T}$, but it is not a null. Channel B ([0.4079 0.8168 0.4079]) is a linear phase channel with a null. The impulse response and the frequency magnitude response of channel B is shown in Figure 4.3 and 4.4, respectively. We observe from Figure 4.4 that channel B has a spectral null at $f = \frac{1}{2T}$. When a

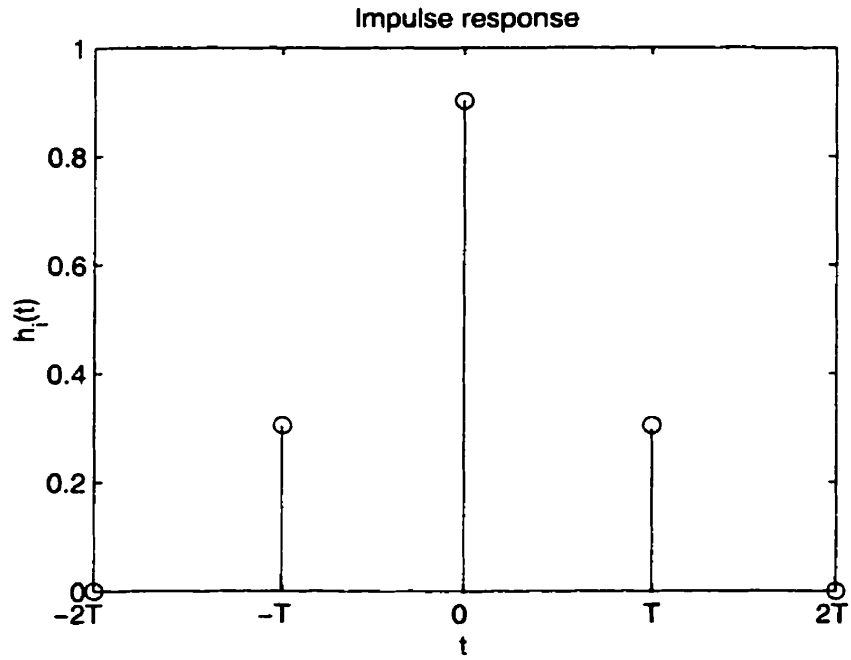


Figure 4.1: Impulse response of channel A

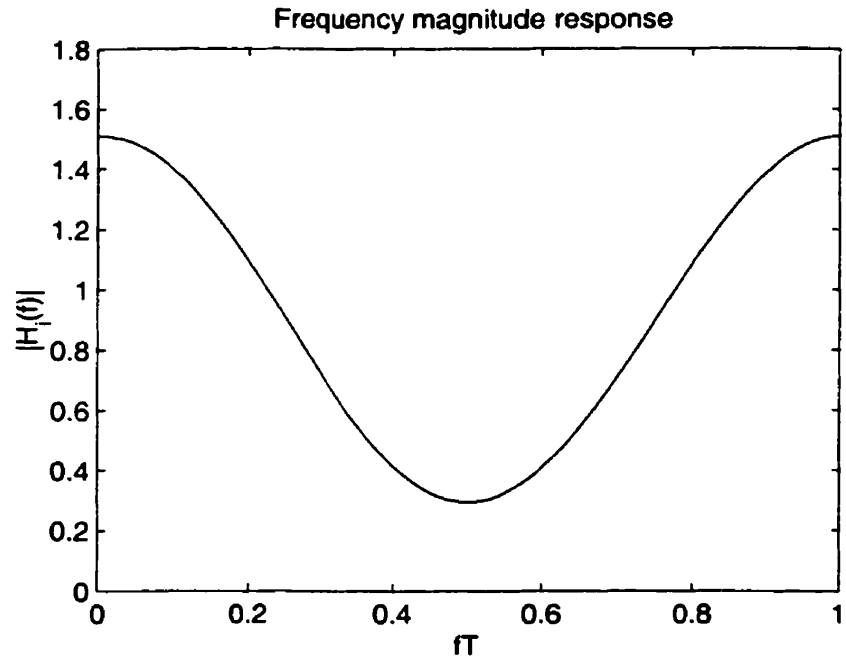


Figure 4.2: Frequency magnitude response of channel A

linear transversal equalizer is used to eliminate ISI, the resulting filter is the inverse of the channel. For channel B, i.e. channel with spectral null, the resulting filter will have large gain at the null region. This amplifies noise in that region and causes more probability of error. Therefore, channel with nulls are more severe than those channels without null. In such channels, DFE is needed.

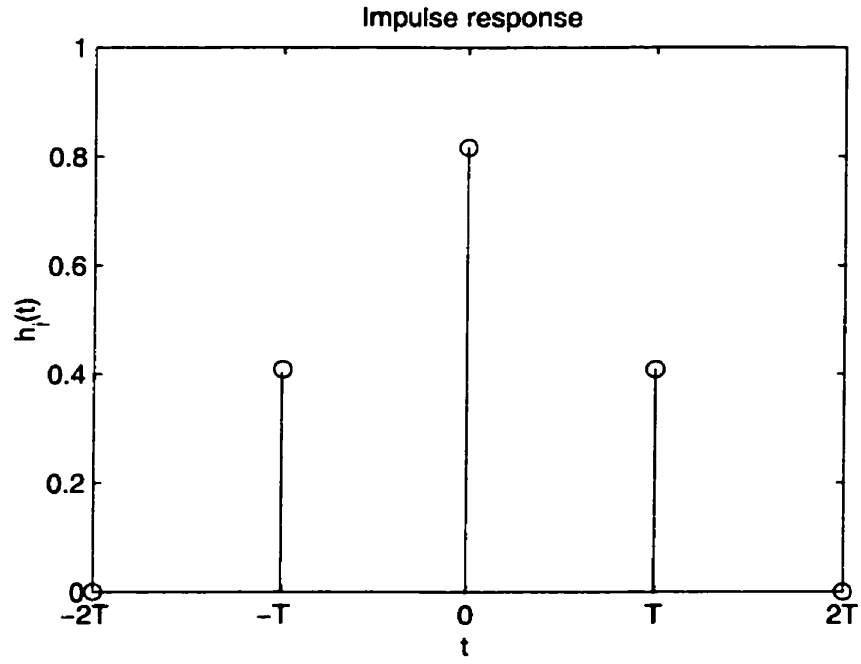


Figure 4.3: Impulse response of channel B

### 4.1.2 Simulation Results

For the simulations, the modified RLS algorithm($w = 0.998$) is used for the adaptation of the NDFE taps. The training sequence is 500 bits long and the actual data is 20000 bits long. The NDFE has 6 taps in the FF filter and 4 taps in the FB filter. Figure 4.5, 4.6, 4.7 and 4.8 show the effects of $\beta$ (at constant $BT = 0.3$) and $BT$ (at constant $\beta = 0.9$) on the proposed noncoherent receiver under channel A and B. The performance of the coherent receiver under each channel is also presented as a reference. From the figures, we verify that channel B is more harsh than channel A.

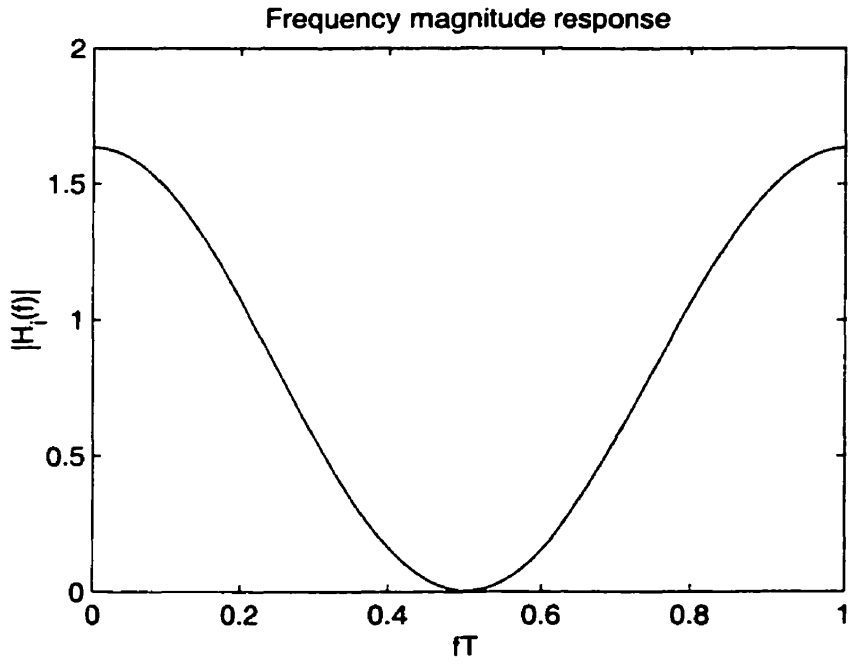


Figure 4.4: Frequency magnitude response of channel B

Yet, the effects of $\beta$ and $BT$ on the receivers under both channels are very similar to the results under the AWGN channel.

## 4.2 Performance Under Rayleigh Fading Channels

### 4.2.1 Rayleigh Fading Channel Model

In Chapter 2, we introduced the multipath fading channel and some of its characteristics. Here, we will look at a popular fading channel model, the Rayleigh fading channel. If the sum of the multipath components is a complex Gaussian process, the magnitude of the process has a Rayleigh distribution. Therefore, in a Rayleigh fading channel, the transmitted signal is randomly modulated with a complex Gaussian process denoted as z(t). The wireless channel in which only one such path exists is known as a flat Rayleigh fading channel. When there are more than one such path existing, the channel is called multipath Rayleigh fading channel. In multipath fad-

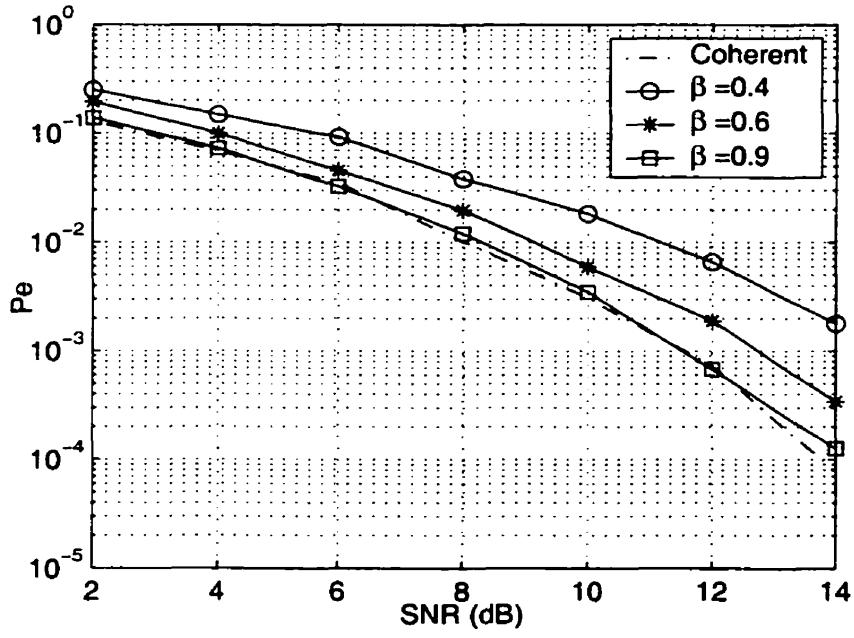


Figure 4.5: Performance of the receiver under channel A with various $\beta$

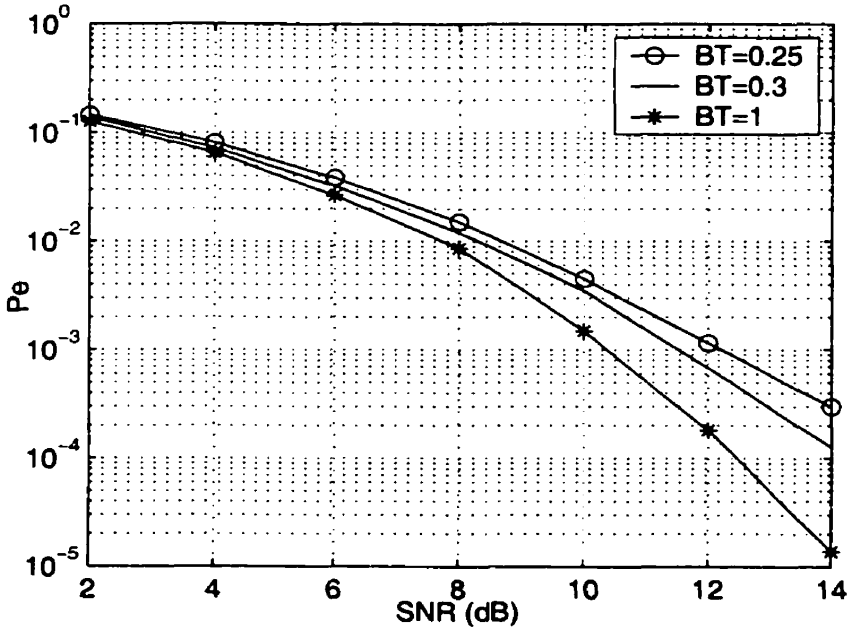


Figure 4.6: Performance of the receiver under channel A with various $BT$

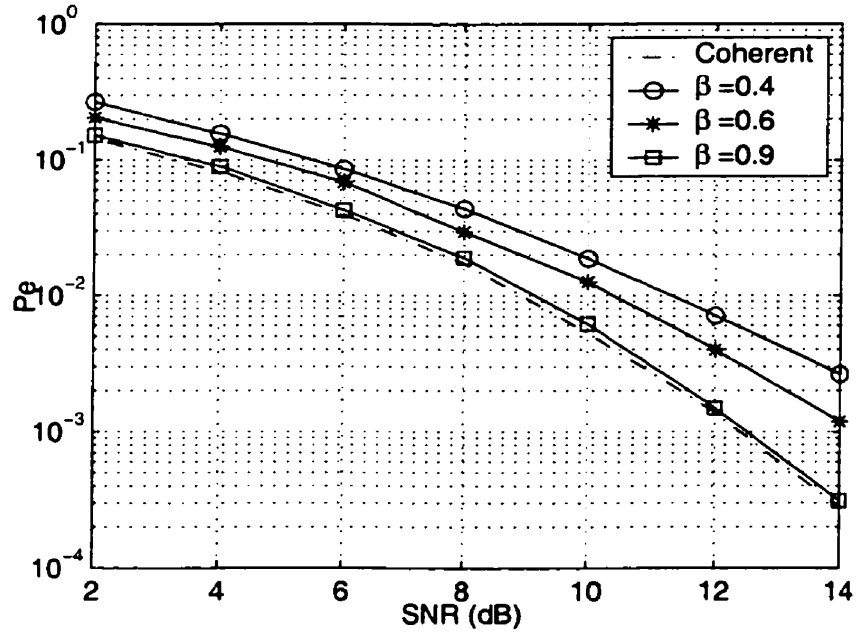


Figure 4.7: Performance of the receiver under channel B with various $\beta$

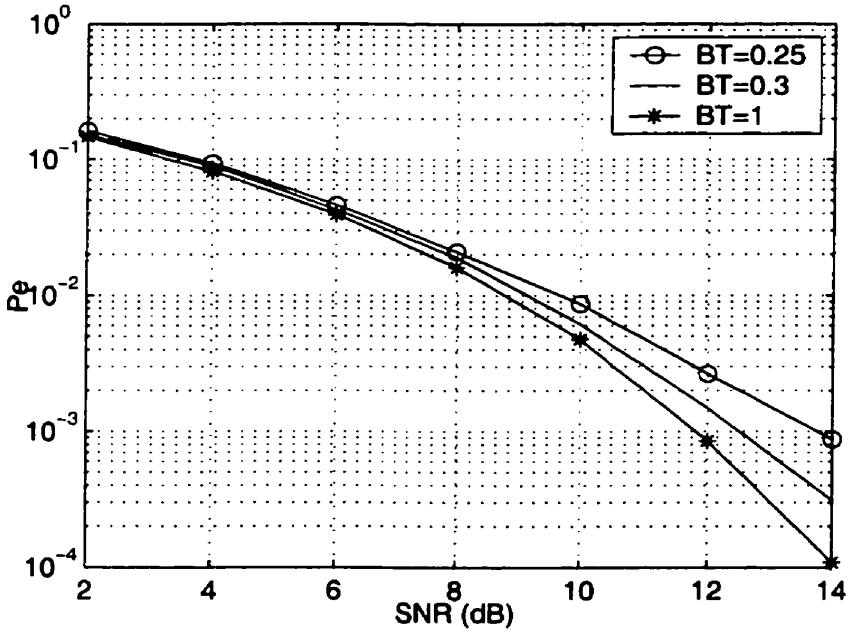


Figure 4.8: Performance of the receiver under channel B with various $BT$

ing channel, if the difference between each path delay, $\tau$, is significant relative to a symbol duration, then there exists frequency selectivity in the channel, which would introduce ISI. A parameter called rms delay spread, $\rho_\tau$, is introduced to indicate the significance of the ISI of the channel. In this thesis, we will use a two ray fading channel model to investigate the effect of $\rho_\tau$ on the proposed receiver. The two ray fading channel model is shown in Figure 4.9. The gain $z_1(t)$ and $z_2(t)$ are independent complex Gaussian processes. The two rays in the channel have the same mean power, so the mean rms delay spread is $\frac{\tau}{2}$.

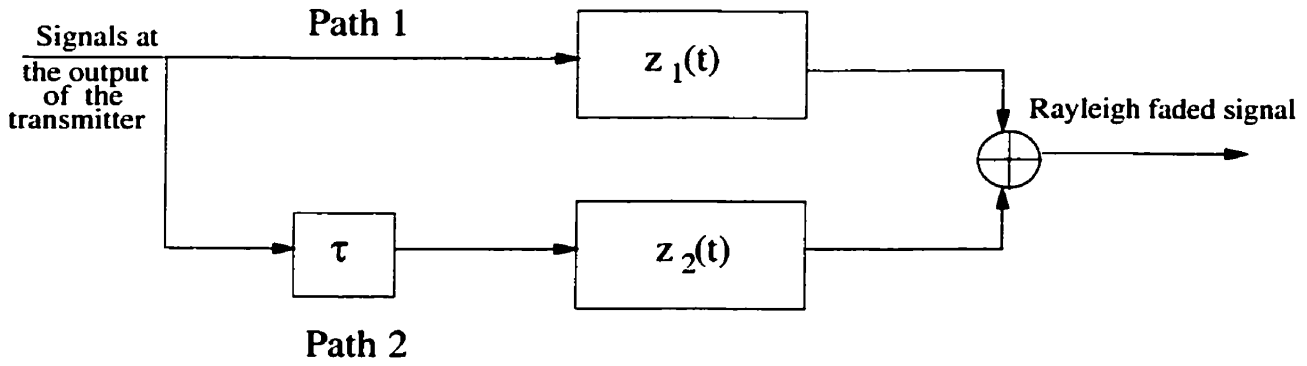


Figure 4.9: The block diagram of a frequency selective Rayleigh fading channel

### 4.2.2 Simulation Results

To simulate Rayleigh distribution, 1000 zero mean, unit variance, complex Gaussian random variables are generated. For the simulations, the modified RLS algorithm($w$ = 0.998) is used for adaptation of NDFE taps. The training sequence is 500 bits long and the actual data is 20000 bits long. The NDFE has 6 taps in the FF filter and 4 taps in the FB filter. Figure 4.10 and Figure 4.11 shows the effects of $\beta$ and $BT$ on the proposed noncoherent receiver under flat Rayleigh fading channel. In Figure 4.10, the performance of noncoherent detection of DBPSK and MSK are also plotted for reference. The probability of error for DBPSK and MSK in flat Rayleigh fading

channel are given as [2]:

$$Pe = \frac{1}{2(1 + E_b/N_0))} \tag{4.5}$$

The figures show that the general trend of the effects of the parameters are similar to the case of the AWGN channel. However, the degree is much reduced. It was mentioned that frequency selective fading, caused by multipath delay spread, causes ISI. If equalizers are not used, the ISI can result in an irreducible BER floor. Figure 4.12 shows the effect of delay spread on the performance of the proposed receiver. It was confirmed through simulation that as $SNR \rightarrow \infty$, there was no BER floor forming with increasing delay spread. When compared to flat Rayleigh fading, because of channel diversity, the performance of the receivers with channel delay spread greater than $0.5T$ are better than the performance of the receiver under flat Rayleigh fading channel.

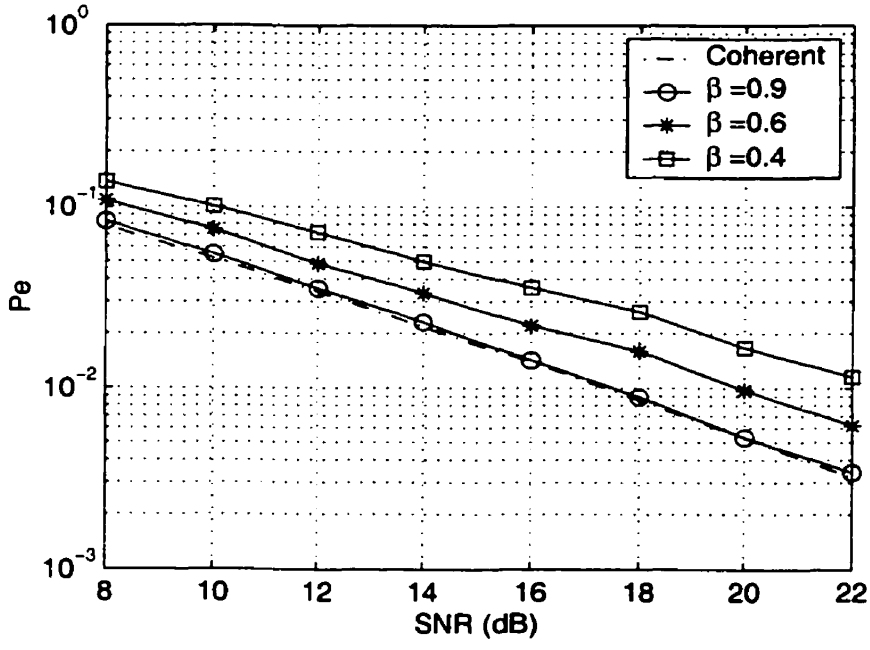


Figure 4.10: Performance of the receiver under flat Rayleigh fading channel with various $\beta$

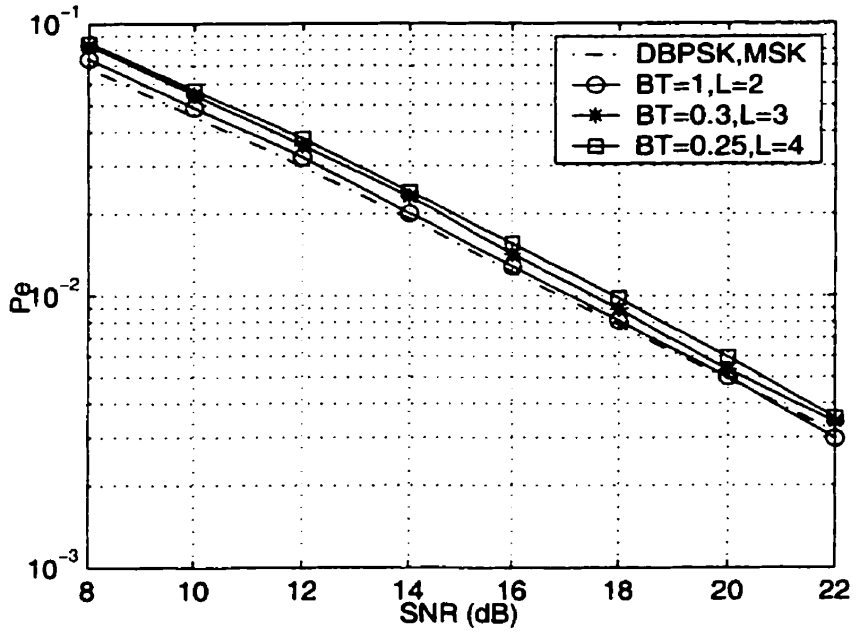


Figure 4.11: Performance of the receiver under flat Rayleigh fading channel with various $BT$

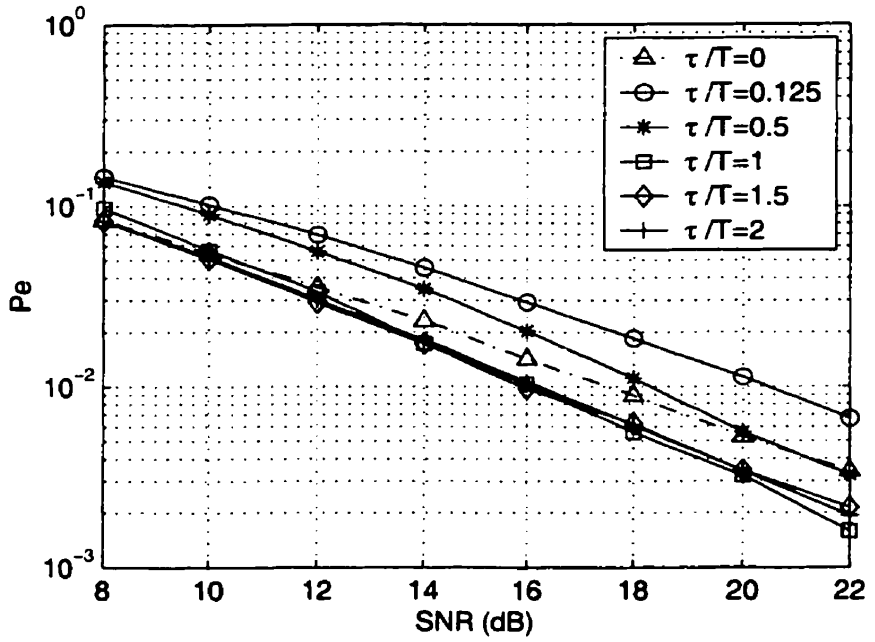


Figure 4.12: Performance of the receiver under multipath Rayleigh fading channel with various $\tau$

# Chapter 5

# Conclusion

## 5.1 Summary of Results

In this thesis, we proposed a reduced complexity noncoherent receiver for GMSK signals. The main body of the thesis is divided in to three parts. In chapter 2, we have given an overview on GMSK, the Laurent representation of CPM, signal detection schemes, fading channel and some typical coherent and noncoherent equalization techniques. In chapter 3, we have investigated the design issues of the noncoherent GMSK receiver based on the Laurent representation under AWGN channel. In chapter 4, we have evaluated the proposed noncoherent receiver in fading channels.

In chapter 2, it was noted that due to its low implementation costs and robustness against frequency and carrier phase offsets, differential detection, a noncoherent signal detection scheme, may be more advantageous over coherent signal detection schemes in fading channel. It was also shown that a coherent Laurent-based MLSE GMSK demodulator requires $4 \times 2^{L-1}$ states in AWGN channel. If channel-induced ISI is also considered, more states must be added. As a result, the overall computational complexity of the receiver will be too high to implement. Therefore, suboptimum channel equalization schemes are used to combat ISI. We learned that under severe fading channel, such as channels with spectral null, DFE is a better suboptimum

equalization technique than LE.

In chapter 3, it was discovered that by using Laurent one-pulse approximation of GMSK and a derotation process, a GMSK system can be well approximated by DBPSK system. Thus, a high performance PSK-based NDFE scheme can be applied directly to GMSK signals. It was shown that the performance of the proposed noncoherent receiver can approach the corresponding coherent GMSK receiver. In addition, it was shown that the proposed noncoherent receiver suffers only about 1.5 dB loss when compared to the optimum coherent GMSK receiver. Two intrinsic parameters (BT and $\beta$) were also examined to see their effects on the performance. Furthermore, the performance of the proposed noncoherent receiver is compared to other known noncoherent GMSK receivers. The result concluded that the proposed receiver has high performance.

In chapter 4, the proposed noncoherent receiver was examined for fading channels. The receivers, along with the two parameters, were first examined under static fading channel with deterministic properties. They were then examined under quasi-static flat Rayleigh fading channels. Finally, the receiver was examined under two-ray Rayleigh fading channels with different multipath delay spread. Figure 5.1 shows that at $\beta = 0.9$ and BT=0.3, the performance were poorer going from AWGN channel to static fading channels then to flat Rayleigh fading channel. It is concluded that in multipath Rayleigh fading channel, due to path diversity, the performance of the receivers with channel delay spread greater than $0.5T$ are better than the performance of the receiver under flat Rayleigh fading channel.

## 5.2 Suggestions for Future Work

We used two ray Rayleigh fading channel model to study the effects of multipath delay spread on the proposed receiver. In a real wireless communication channel, there are greater number of rays. Therefore, more accurate fading channel models can be used

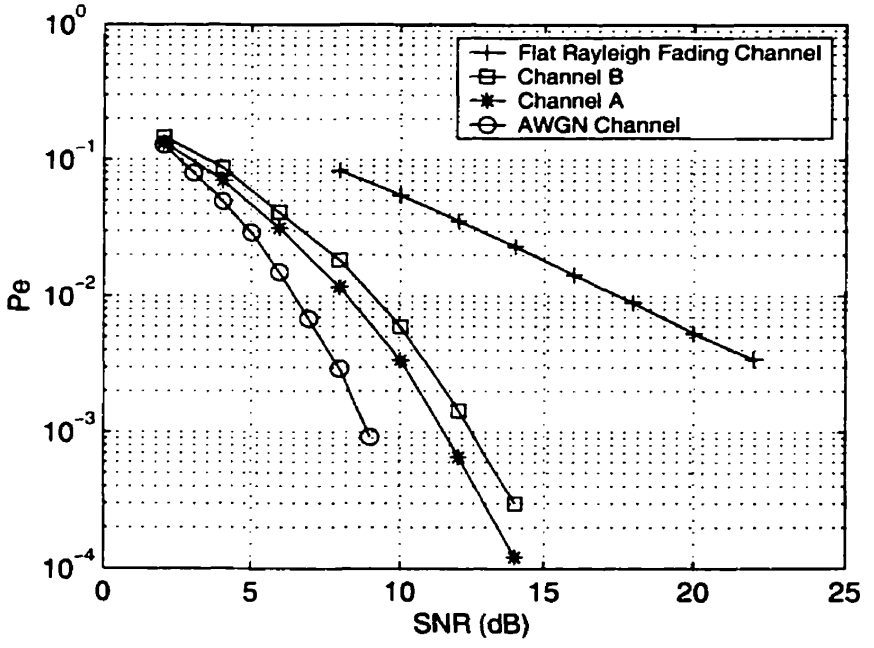


Figure 5.1: BER Performances of the proposed noncoherent receiver at $\beta = 0.9$ under various channels

to further evaluate the receiver. In addition, instead of simulated fading channels, real fading channels may be used to evaluate the performance of the proposed receiver. This could be done by using measured channel responses.

In a practical wireless communication systems, channel coding is usually used to improve the performance of the overall system. Furthermore, adding an error-correcting code involves finding a balance between the strength of the code chosen and the complexity involved in encoding and decoding it. Therefore, it is worthwhile to investigate the performance gain on the proposed noncoherent receiver by using various coding schemes.

# Appendix A

# Derivation of NDFE Decision Rule

In this appendix, the decision rule for schober's NDFE scheme is derived. This derivation is drawn heavily from [29].

## A.1 Transmission Model

Figure A.1 shows a block diagram of the discrete-time transmission model. All signals are represented by their complex-valued baseband equivalents. At the transmitter, the MDPSK symbols a[k] are differentially encoded. The resulting MPSK symbol b[k] are given by

$$b[k] = a[k]b[k-1], \qquad k = 1, 2, ... \tag{A.1}$$

The received signal, sampled at time kT at the output of the receiver input filter can written as

$$r[k] = e^{j\theta} \sum_{\nu=0}^{L_h-1} h_\nu b[k-\nu] + n[k] \tag{A.2}$$

where $\Theta$ denotes an unknown, constant, uniformly distributed phase introduced by the channel. $h_\nu, 0 \leq n \leq L_h - 1$, are the coefficients of the combined discrete-time impulse response of the transmit filter, channel, and receiver input filter;its length is denoted by $L_h$. $n[k]$ is the $n(t)$ represents complex additive Gaussian noise with a one-sided power spectral density of $N_0$.

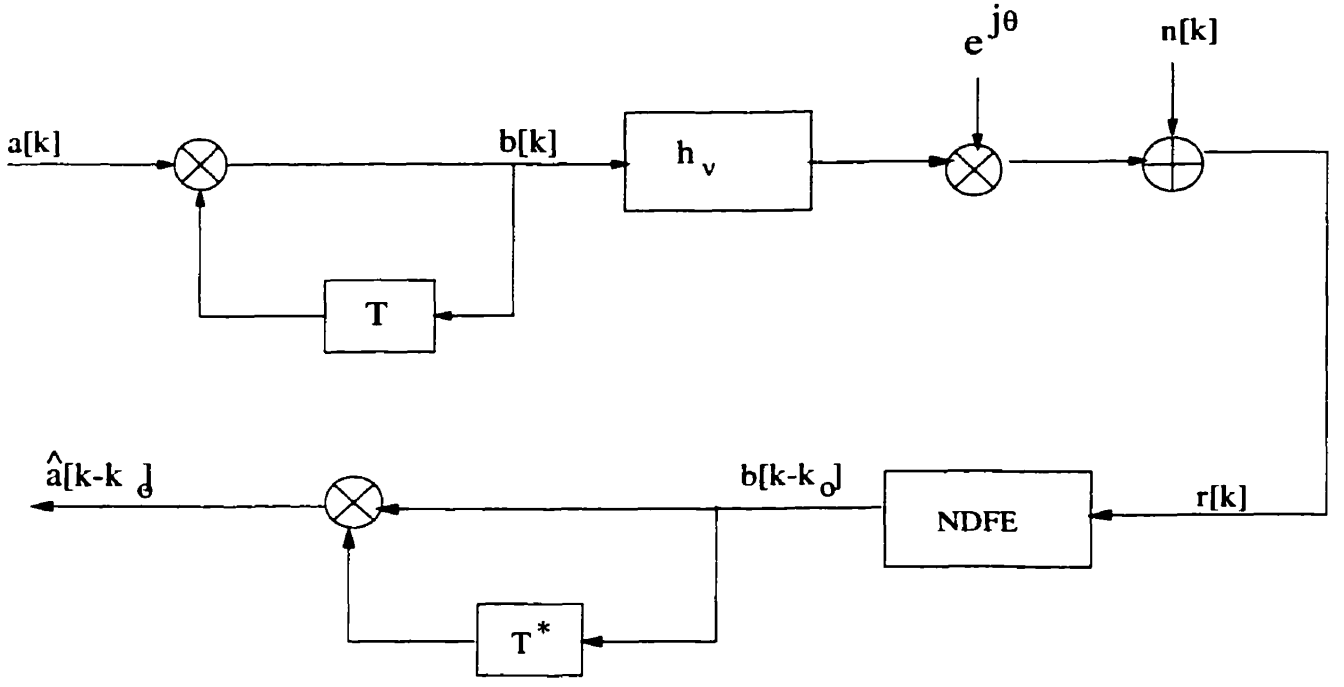


Figure A.1: Block diagram of the discrete-time transmission model for MPSK signals

## A.2 NDFE Decision Rule

Based on observation of N received symbols $r[k-\nu], 0 \leq \nu \leq N-1$, the optimum noncoherent MLSE metric for estimation of a block of $N \geq 2$ symbols $b[k-\nu]$ is given in [16]. For moderate to high $E_s/N_0$ ratios, the optimum metric is well approximated by [16]

$$\lambda[k] \triangleq \sum_{\nu=k-N+1}^{k} (\mid r[\nu] \mid^2 + \mid y[\nu] \mid^2) - 2 \left| \sum_{\nu=k-N+1}^{k} r[\nu] y^*[\nu] \right| \tag{A.3}$$

where

$$y[k] \triangleq \sum_{\nu=0}^{L_h-1} h_\nu b[k-\nu] \tag{A.4}$$

The feedforward(FF) filter of the NDFE is defined as $f_{F,\nu}[k], 0 \leq \nu \leq L_F - 1$. The FF filter output signal can be written as

$$r_{DFE}[k] = f_F^H[k] R[k] \tag{A.5}$$

where $[]^H$ denotes Hermitian transposition and

$$R[k] \triangleq [r[k]\ r[k-1]\ ...\ r[k-L_F+1]]^T$$

The feedback(FB) filter of the NDFE is defined as $f_{B,\nu}[k], 0 \leq \nu \leq L_B - 1$. The FB filter output signal can be written as

$$y_{DFE}[k] = \sum_{\nu=0}^{L_B-1} f_{B,\nu}[k] b[k-k_0-\nu] \tag{A.6}$$

Since FF and FB filters introduce an additional degree of design freedom, we set $f_{B,0}[k] \equiv 1$, thus

$$f_B[k] \triangleq [1\ f_{Bs}[k] \tag{A.7}$$

If we replace $r[k]$ with $r_{DFE}[k]$ and $y[k]$ with $y_{DFE}[k]$, the FF and FB filter coefficients can be adjusted to minimize the variance of the difference between detector input signal and transmitted symbol. Thus, A.3 becomes the following suboptimum metric

$$\lambda[k] = \sum_{\nu=k-N+1}^{k} (\mid r_{DFE}[\nu] \mid^2 + \mid y_{DFE}[\nu] \mid^2) - 2\mid \sum_{\nu=k-N+1}^{k} r_{DFE}[\nu] y^*_{DFE}[\nu] \mid \tag{A.8}$$

If we interpret NDFE as noncoherent reduced-state MLSE with only one state, in A.7, the unknown symbols $b[k-k_0-\nu], \nu \geq 1$, has to be replaced by previously decided symbols $\hat{b}[k-k_0-\nu], \nu \geq 1$. The resulting metric to be minimized with respect to $b[k-k_0]$ is

$$\begin{aligned}
\hat{\lambda}[k] \ = \ & \sum_{\nu=k-N+1}^{k} \mid r_{DFE}[\nu] \mid^2 + \mid b[k-k_0] + f^H_{Bs}[k]\hat{c}[k-k_0-1] \mid^2 \\
+ \ & \sum_{\nu=k-N+1}^{k-1} \mid \hat{y}_{DFE}[\nu] \mid^2 - 2 \mid r_{DFE}[k](b[k-k_0] + f^H_{Bs}[k]\hat{c}[k-k_0-1])^* \\
+ \ & \sum_{\nu=k-N+1}^{k-1} r_{DFE}[\nu]\hat{y}^*_{DFE}[\nu] \mid
\end{aligned} \tag{A.9}$$

where

$$\hat{y}_{DFE}[k] = \sum_{\nu=0}^{L_B-1} f_{B,\nu}[k]\hat{c}[k-k_0-\nu]$$

$$\hat{c}[k-k_0-1] \triangleq [\hat{b}[k-k_0-1]\ \hat{b}[k-k_0-2]\ ...\ \hat{b}[k-k0-L_B+1]]^T$$

Since the additive terms in A.9 do not influence the decision, they are omitted. The resulting DFE decision rule is then given by equation 3.14 in chapter 3.

# Appendix B

# Modified RLS algorithm

In this appendix, a modified RLS algorithm is presented[29]. It is used to minimize the noncoherent cost function defined in Chapter 3. The feedforward filter coefficient may be calculated by using the following equations:

$$k_F[k] = \frac{P_F[k-1]r[k]}{w + r^H[k]P_F[k-1]R[k]} \tag{B.1}$$

$$\xi_F[k] = \frac{q_{rec}[k]}{\mid q_{rec}[k] \mid}\hat{y}_{DFE}[k] - f_F^H[k-1]R[k] \tag{B.2}$$

$$f_F[k] = f_F[k-1] + k_F[k]\xi_F^*[k] \tag{B.3}$$

$$P_F[k] = \frac{1}{w}P_F[k-1] - \frac{1}{w}k_F[k]R^H[k]P_F[k-1] \tag{B.4}$$

where $0 \leq w \leq 1$, denotes the forgetting factor of the modified RLS algorithm. The feedback filter coefficient may be calculated similarly as:

$$k_B[k] = \frac{P_B[k-1]\hat{c}[k-k_0-1]}{w + \hat{c}^H[k-k_0-1]P_B[k-1]\hat{c}[k-k_0-1]} \tag{B.5}$$

$$\begin{aligned}\xi_B[k] &= \frac{(q_{rec}[k])^*}{\mid q_{rec}[k] \mid}r_{DFE}[k] - b[k-k_0] \\ &- f_B^H[k-1]\hat{c}[k-k_0-1]\end{aligned} \tag{B.6}$$

$$f_B[k] = f_B[k-1] + k_B[k]\xi_B^*[k] \tag{B.7}$$

$$P_B[k] = \frac{1}{w}P_B[k-1] - \frac{1}{w}k_B[k]\hat{c}^H[k-k_0-1]P_B[k-1] \tag{B.8}$$

Similarly to the modified LMS algorithm, it is different from the conventional LMS by the factors $\frac{q_{rec}[k]}{|q_{rec}[k]|}$ and $\frac{q^*_{rec}[k]}{|q_{rec}[k]|}$ for calculation of $\xi_F[k]$ and $\xi_B[k]$.

For initialization of $P_F[0]$ and $P_B[0]$, it is proposed

$$P_X[0] = \frac{1}{\delta_{RLS}} I_{L_Q \times L_Q}, \quad Q = F, B \tag{B.9}$$

$\delta_{RLS}$ is a small positive constant(typical value:0.001) and $I$ is the identity matrix.

The modified RLS algorithm provides a faster convergence than the modified LMS algorithm. Figure B.1 and B.2 compares the learning curves of the modified LMS and RLS algorithms for the noncoherent GMSK(BT=0.3) receiver receiving GMSK signals. The average is done over 500 adaptation processes at $SNR = 8dB$ with $\beta = 0.6$. For LMS, $\delta = 0.03$ is used. For RLS, $w = 0.98$ is used.

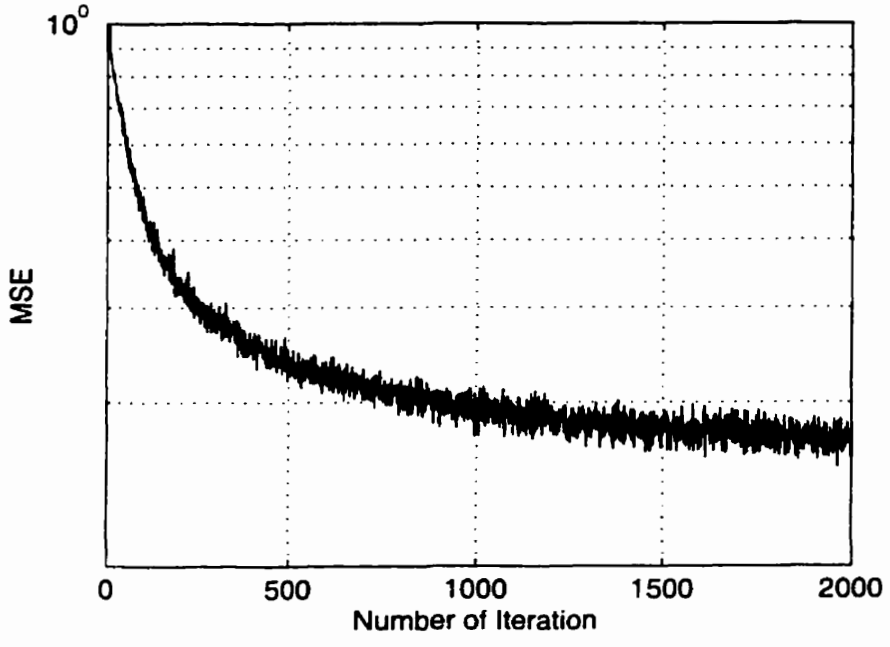


Figure B.1: Learning curve for modified LMS algorithm

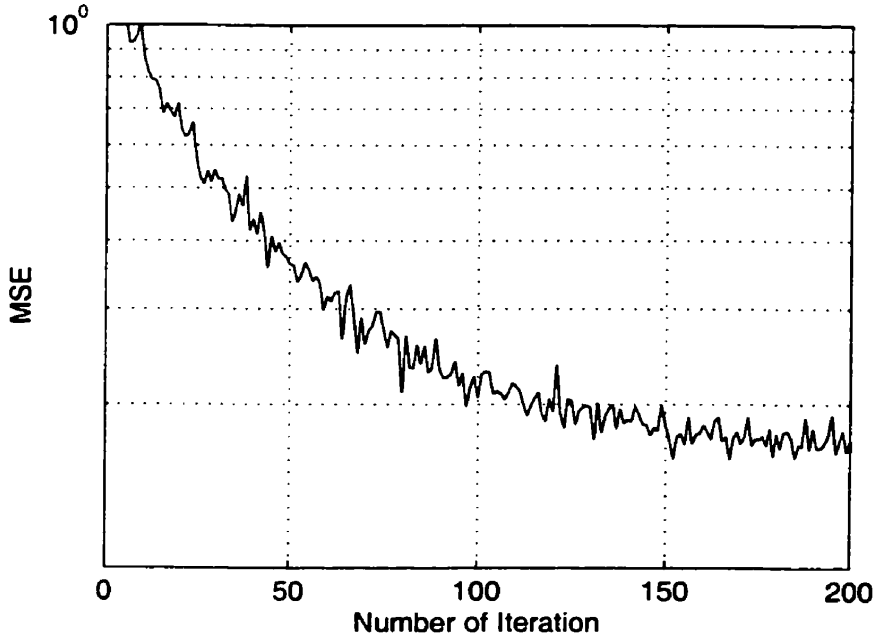


Figure B.2: Learning curve for modified RLS algorithm

# Bibliography


[1] J. Anderson, T. Aulin, C. Sundberg, *Digital Phase Modulation*, New York: Plenum Press, 1986.

[2] J.G. Proakis, *Digital Communications*, Third Edition,New York: McGraw-Hill, Inc., 1995.

[3] S.U.H. Qureshi, "Adaptive Equalization", *Proceedings of the IEEE, Vol. 73, No. 9, Sept. 1985.*

[4] B. Sklar, "Rayleigh Fading Channels in Mobile Digital Communication Systems Part I: Characterization", *IEEE Communication Magazine, pp.90-100, July 1997*

[5] T.S. Rappaport, *Wireless Communication*, New Jersey: Pretice-Hall, Inc., 1995

[6] K. Murota and H. Hirade, "GMSK Modulation for Digital Mobile Radio Telephony", *IEEE Trans. on Communications, Vol. 29, No. 7, pp.1044-1050, July 1981.*

[7] S. Pasupathy, "Minimum Shift Keying: A spectrally Efficient Modulation", *IEEE Communication Magazine, pp.14-22, July 1979.*

[8] Z. Ding and G. Li, "Linear Blind Channel Equalization for GSM Systems", *IEEE ICC 98, Conference Record, Vol. 1, pp.355-359, 1998.*

[9] F. Davarian, "Mobile Digital Communication via Tone Calibration", *IEEE Trans. on Vehicular Technology, Vol. 36, No. 2, pp.55-61, May 1987.*

[10] M.K. Simon and C. C. Wang, "Differential Versus Limiter-Discriminator Detection of Narrow-Band FM", *IEEE Trans. on Communications, Vol. Com-31, No. 11, pp.1227-1234, Nov. 1983.*

[11] M.A. Wickert and W.S. Sward, "Limiter Discriminator-Detected GMSK with FM and GMSK Interference in a Land Mobile Channel", *IEEE Trans. on Communications, Vol. 47, No. 11, pp.1693-1700, Nov. 1999.*

[12] D. Divsalar and M.K. Simon, "Multiple-Symbol Differential Detection of MPSK", *IEEE Trans. on Communications, Com-38, pp.300-308, March 1990.*

[13] M.S. El-Tanany, H.P. Stern and S.A. Mahmoud, "Data Detection and Timing Recovery for a Noncoherent Discriminator-Based GMSK Receiver", *IEEE Vehicular Technology Conference 89, Vol. 1, pp.243-248, 1989.*

[14] S.M. Elnoubi, "Analysis of GMSK with Differential Detection in Land Mobile Radio Channels", *IEEE Trans. on Vehicular Technology, Vol. 35, No. 4, pp.162-167, Nov. 1986.*

[15] A. Yongacoglu and D. Makrakis, "Differential Detection of GMSK using Decision Feedback", *IEEE Trans. on Communications, Vol. 36, No. 6, pp.641-649, June 1988.*

[16] W. Gerstacker, R. Schober and J. B. Huber, "Noncoherent Equalization Algorithms Based on Sequence Estimation", *IEEE GLOBECOM 1998, Vol. 6, pp.3485 -3490, 1998*

[17] F. G. Stremler, *Introduction to Communication Systems*, Third Edition, New York: Addison-Welsley Publishing Company, Inc., 1992.

[18] K. Hirade, M. Ishizuka, F. Adachi and K. Ohtani, "Error-Rate Performance of Digital FM with Differential Detection in Land Mobile Radio Channels", *IEEE Trans. on Vehicular Technology, Vol. 28, No. 3, pp.204-212, August 1919.*

[19] D.A. Johnson, S.W. Wales and P.H. Waters, "Equalizers for GSM", *IEE Colloquium on Methods of Combating Multipaths, pp.1-6, 1990*

[20] J. Tellado-Mourelo and E.K. Welsel, "Adaptive DFE for GMSK in Indoor Radio Channels", *IEEE Journal on Selected Areas in Communication, Vol. 14, No. 3, pp.492-501, April 1996.*

[21] D.D. Falconer, "Application of passband decision equalization in two-dimensional data communication system", *IEEE Transaction on Communication, Vol. 24, pp.1159-1166, Oct 1976.*

[22] H. Zou, H.J. Kim, S. Kim, B. Daneshrad, R. Wesel and W. Magione-Smith, "Equalized GMSK, equalized QPSK and OFDM, a comparative study for high-speed wireless indoor data communications", *49th Vehicular Technology Conference, Vol. 2, pp.1106 -1110, 1999*

[23] F. Adachi and K. Ohno, "Performance Analysis of GMSK Frequency Detection with DFE in Digital Land Mobile Radio", *IEE Proceeding, Vol. 135, Pt. F, No. 3, pp.199-207, June 1988.*

[24] T. Kohama, H. Kondoh and Y. Akaiwa, "An Adaptive Equalizer for Frequency-Selective Mobile Radio Channels with Noncoherent Demodulation", *41st IEEE Vehicular Technology Conference, pp.770 -775, 1991.*

[25] N. Benvenuto, R. Corvaja, and L. Tomba, "Diversity Selection Combining and Nonlinear Equalization in DQPSK indoor Radio System", *Proceedings of IEEE Communication Theory Mini-Conference in Conjunction with Globecom 94, pp.100-103, 1994.*

[26] M.J. Smith, C.F.N. Cowan, and P.F. Adams, "Nonlinear Echo Cancellers Based on Transpose Distributed Arithmetic", *IEEE Transaction on Circuits and Systems, Vol.35, no. 1, pp.6-18, 1988.*

[27] A. Masoomzadeh-Fard and S. Pasupathy, "Nonlinear Equalization of Multipath Fading Channel with Noncoherent Demodulation", *IEEE Journal on Selected Areas in Communication, Vol. 14, No. 3, pp.512-520, April 1996.*

[28] A.E. Jones and R. Perry, "Frequency-offset Invariant Equalizer for Broadband Wireless Networks", *The Ninth IEEE International Symposium on Personal, Indoor and Mobile Radio Communications 98, Vol. 1, pp.33-37, 1998.*

[29] R. Schober and W.H. Gerstacker, "Adaptive Noncoherent DFE for MDPSK Signals Transmitted Over ISI Channels", *IEEE Transactions on Communications, Vol. 48, pp.1128-1140, July 2000.*

[30] R. Schober, W.H. Gerstacker and J.B. Huber "Adaptive Linear Equalization Combined With Noncoherent Detection for MDPSK Signals", *IEEE Transactions on Communications, Vol. 48, pp.733-738, May 2000.*

[31] P. A. Laurent, "Exact and Approximate Construction of Digital Phase Modulations by Superposition of Amplitude Modulated Pulses (AMP)", *IEEE Transactions on Communications, Vol. Com-34, No. 2, pp.150-160, Feb. 1986.*

[32] L. Chen,"Reduced-Complexity Coded GMSK System Using Iterative Decoding", *M.A.Sc. thesis, Toronto, Ont: University of Toronto, 2000.*

[33] G.K. Kaleh, "Simple Coherent Receivers for Partial Response Continuous Phase Modulation", *IEEE Journal on Selected Areas in Communications, Vol. 7, pp.1427-1436, Dec. 1989.*

[34] G. Li and Z. Ding, "Blind Linear Equalization for GMSK Signals in a Mobile Environment", *IEEE Wireless Communications and Networking Conference 99, Vol. 2, pp. 801-804, 1999.*

[35] N. Al-Dhahir and G. Saulnier, "A High Performance Reduced-complexity GMSK Demodulator", *IEEE Transactions on Communications, Vol. 46, No. 11, pp.1409-1412, Nov. 1998.*

[36] J. Feuerstein, "Performance of Decision Feedback Equalizers in Simulated Urban and Indoor Radio Channels", *IEICE Transaction on Communication, Vol. E76-B, No.2, pp. 78-89, Feb. 1993.*

[37] S.M. Kay, *Modern Spectral Estimation,* Prentice Hall, 1988.

[38] I. Korn, "GMSK with Limiter Discriminator Detection in Satellite Mobile Channel", *IEEE Transactions on Communications, Vol. 39, No. 1, pp.94-100, Jan. 1991.*

[39] G. Colavolpe and R. Raheli, "Noncoherent Sequence Detection of CPM", *Electronics Letters, Vol. 34, No. 3, pp.259-261, 5th Feb. 1998.*